The Heating and Cooling of Coronal Loops

Markus J. Aschwanden (LMSAL)

credit :

Harry P. Warren & Ignacio Ugarte-Urra (NRL)

Second Hinode Science Meeting - 29 Sept - 3 Oct 2008, Boulder, CO

http://www.lmsal.com/~aschwand/ppt/2008_Hinode_Boulder.ppt

Equilibrium models of coronal loops

A 1-D hydrostatic solution of a coronal loop fulfills the momentum and energy equation

$$\frac{dp(s)}{ds} - \frac{dp_{grav}(s)}{dr}\left(\frac{dr}{ds}\right) = 0$$

$$p(s) = 2n_e(s)k_B T_e(s)$$

$$E_H(s) - E_R(s) - \frac{1}{A(s)}\frac{d}{ds}A(s)F_C(s) = 0$$

Heating function:

$$E_H(s) = ...?$$

Energy loss by radiation:

$$E_R(s) = n_e^2(s)\Lambda(T)$$

Energy loss by thermal conduction flux:

$$F_C(s) = -\kappa T^{5/2}(s)\frac{dT(s)}{ds}$$

RTV solution: T(s), n(s)

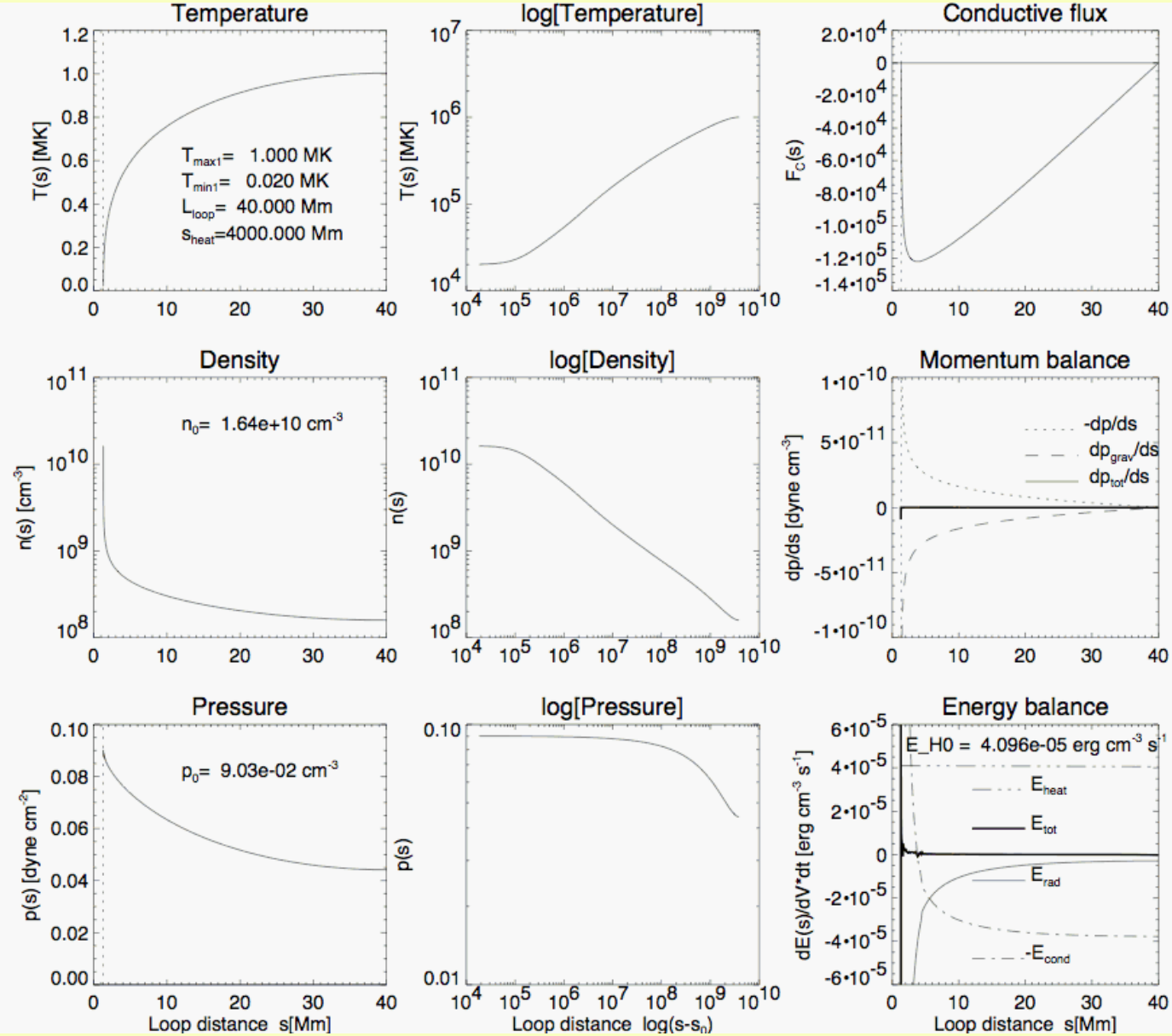

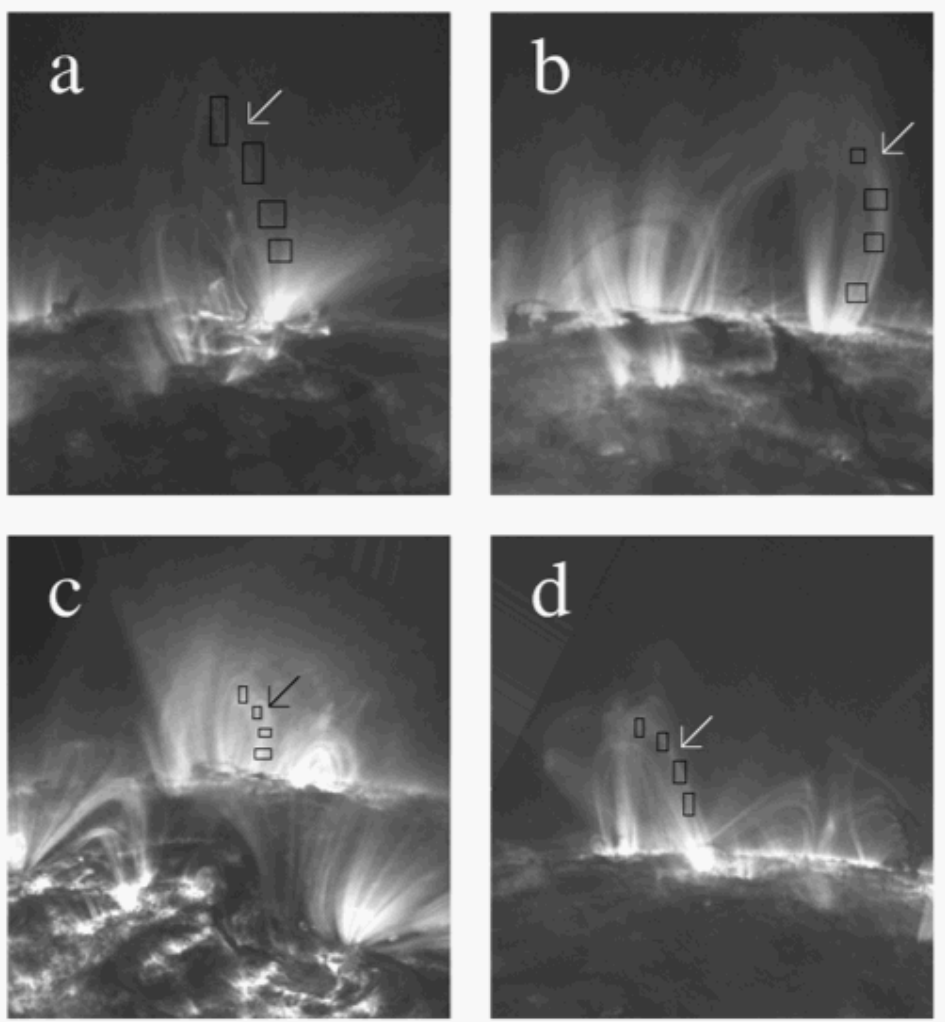

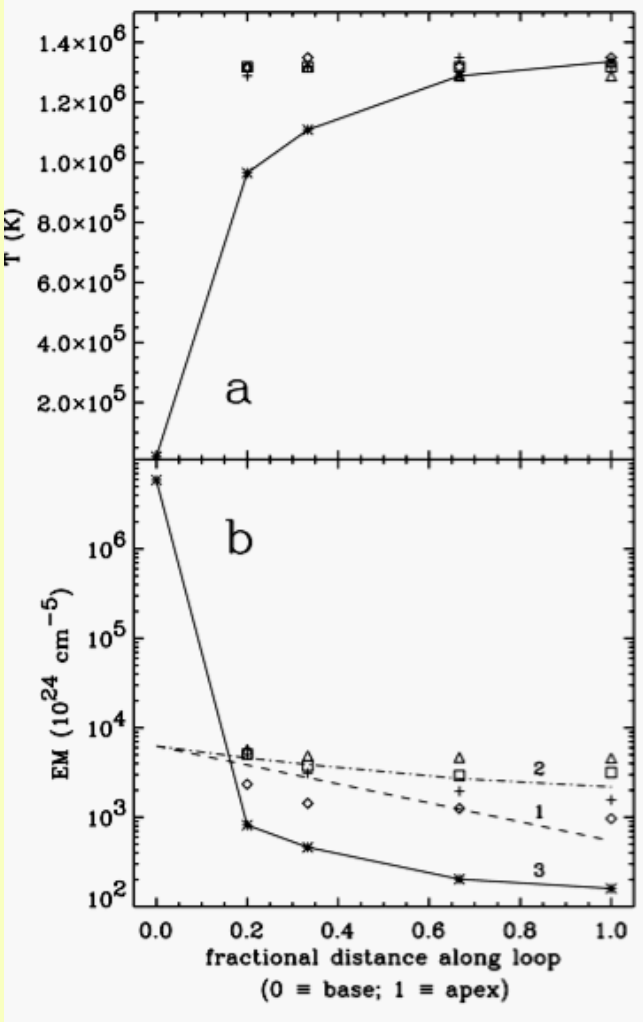

TRACE observations show loops with higher densities and flatter temperature profiles than predicted by RTV (Lenz et al. 1999)

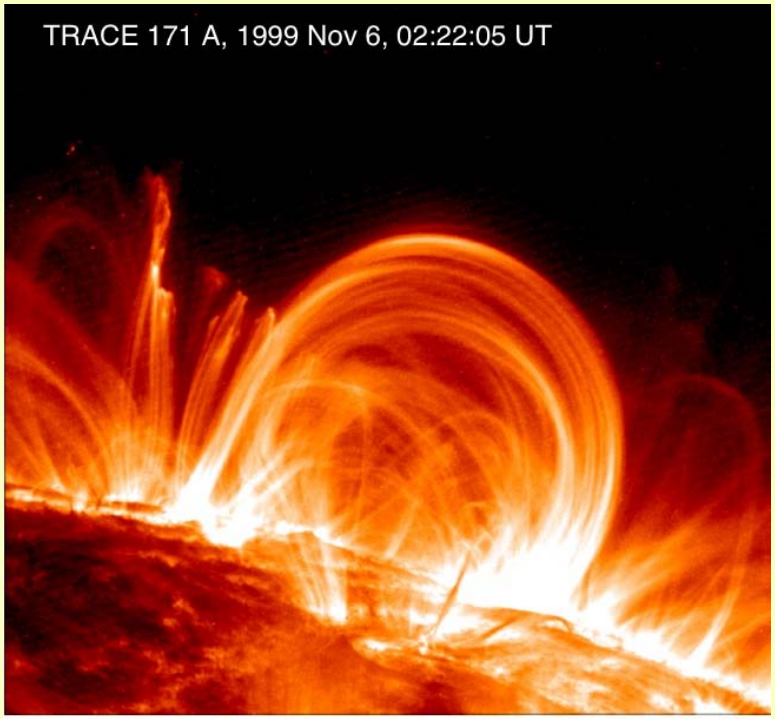

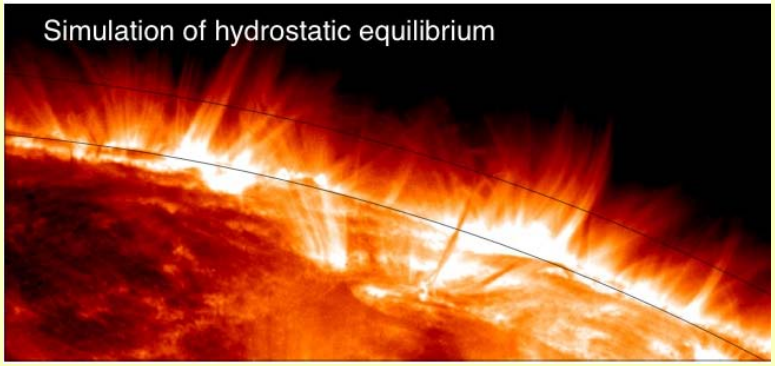

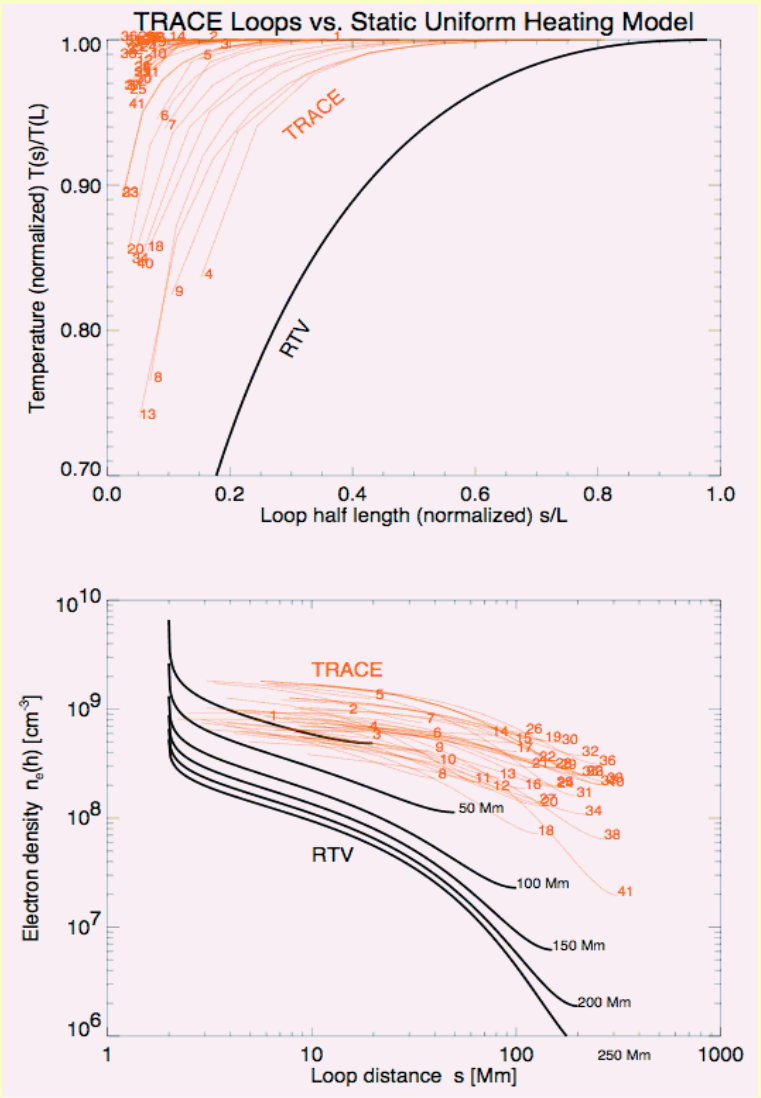

TRACE reveals overdensities and flatter temperature profiles than predicted by RTV

(Aschwanden, Nightingale, & Alexander 2000)

Hydrostatic equilibrium solutions were generalized for non-uniform heating and gravitational stratification (Serio et al. 1981)

$$T_{\max} = 1400 (p_0 L)^{1/3} \exp\left(-0.08 \frac{L}{s_H} - 0.04 \frac{L}{\lambda_p} \right),$$

$$E_{H0} = 0.95 \times 10^{-6} T_{\max}^{7/2} L^{-2} \exp\left(0.78 \frac{L}{s_H} - 0.36 \frac{L}{\lambda_p} \right)$$

The RTVS solutions can produce higher densities and flatter temperature profiles - Does this solution match the observed coronal EUV loops ?

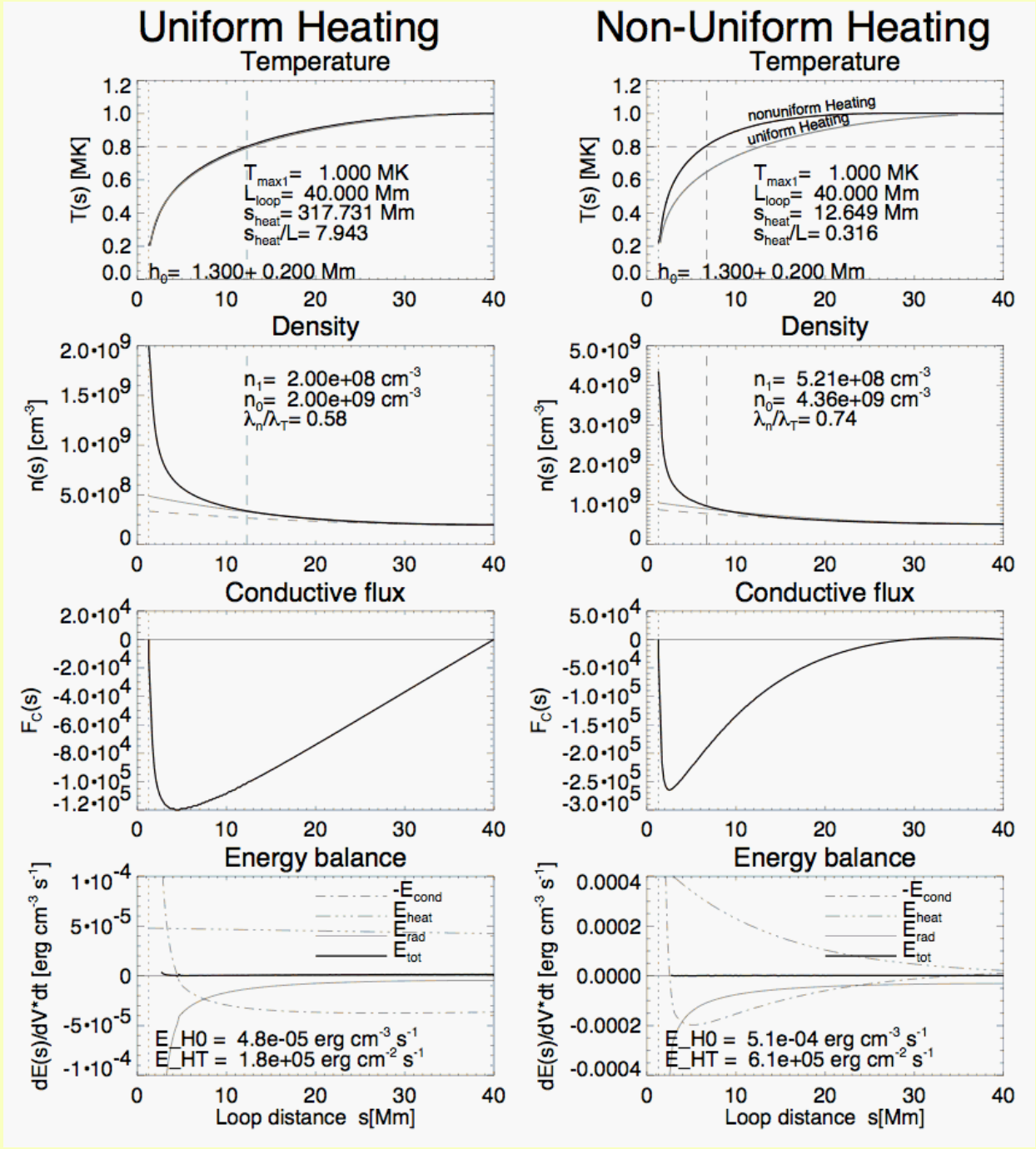
Uniform Heating
Temperature
T(s) [MK]
T_{max1}= 1.000 MK
L_{loop}= 40.000 Mm
s_{heat}= 317.731 Mm
s_{heat}/L= 7.943
h_0= 1.300+ 0.200 Mm
Density
n(s) [cm^{-3}]
n_1= 2.00e+08 cm^{-3}
n_0= 2.00e+09 cm^{-3}
λ_n/λ_T= 0.58
Conductive flux
$F_C(s)$
Energy balance
dE(s)/dV*dt [erg cm^{-3} s^{-1}]
$-E_{cond}$
E_{heat}
E_{rad}
E_{tot}
E_H0 = 4.8e-05 erg cm^{-3} s^{-1}
E_HT = 1.8e+05 erg cm^{-2} s^{-1}
Loop distance s[Mm]
Non-Uniform Heating
Temperature
nonuniform Heating
uniform Heating
T(s) [MK]
T_{max1}= 1.000 MK
L_{loop}= 40.000 Mm
s_{heat}= 12.649 Mm
s_{heat}/L= 0.316
h_0= 1.300+ 0.200 Mm
Density
n(s) [cm^{-3}]
n_1= 5.21e+08 cm^{-3}
n_0= 4.36e+09 cm^{-3}
λ_n/λ_T= 0.74
Conductive flux
$F_C(s)$
Energy balance
dE(s)/dV*dt [erg cm^{-3} s^{-1}]
$-E_{cond}$
E_{heat}
E_{rad}
E_{tot}
E_H0 = 5.1e-04 erg cm^{-3} s^{-1}
E_HT = 6.1e+05 erg cm^{-2} s^{-1}
Loop distance s[Mm]

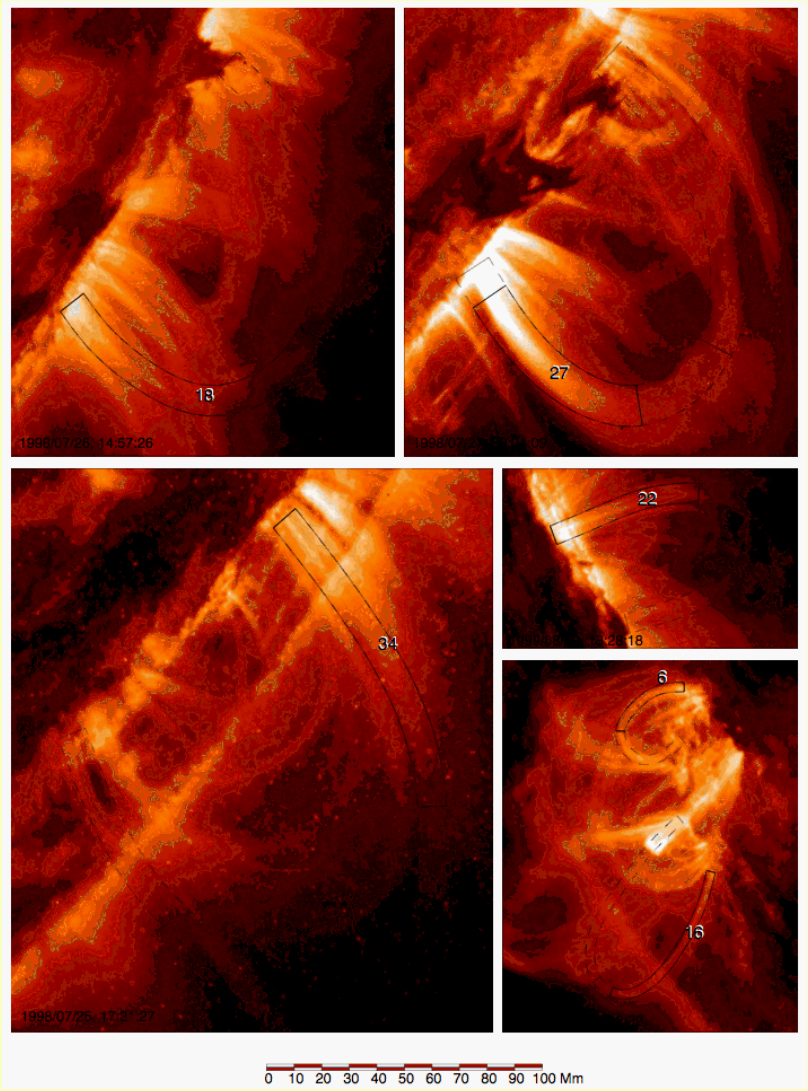

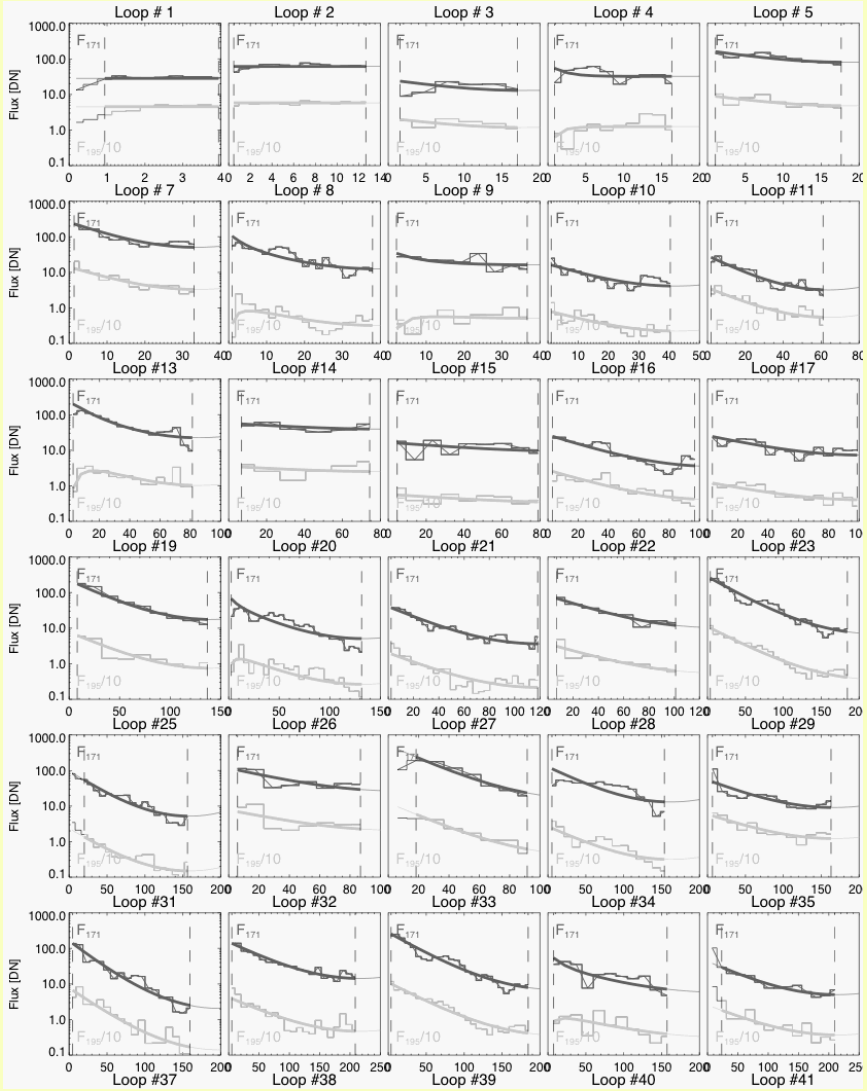

The observed TRACE 171 & 195 flux profiles can be fitted with Serio's model, but …

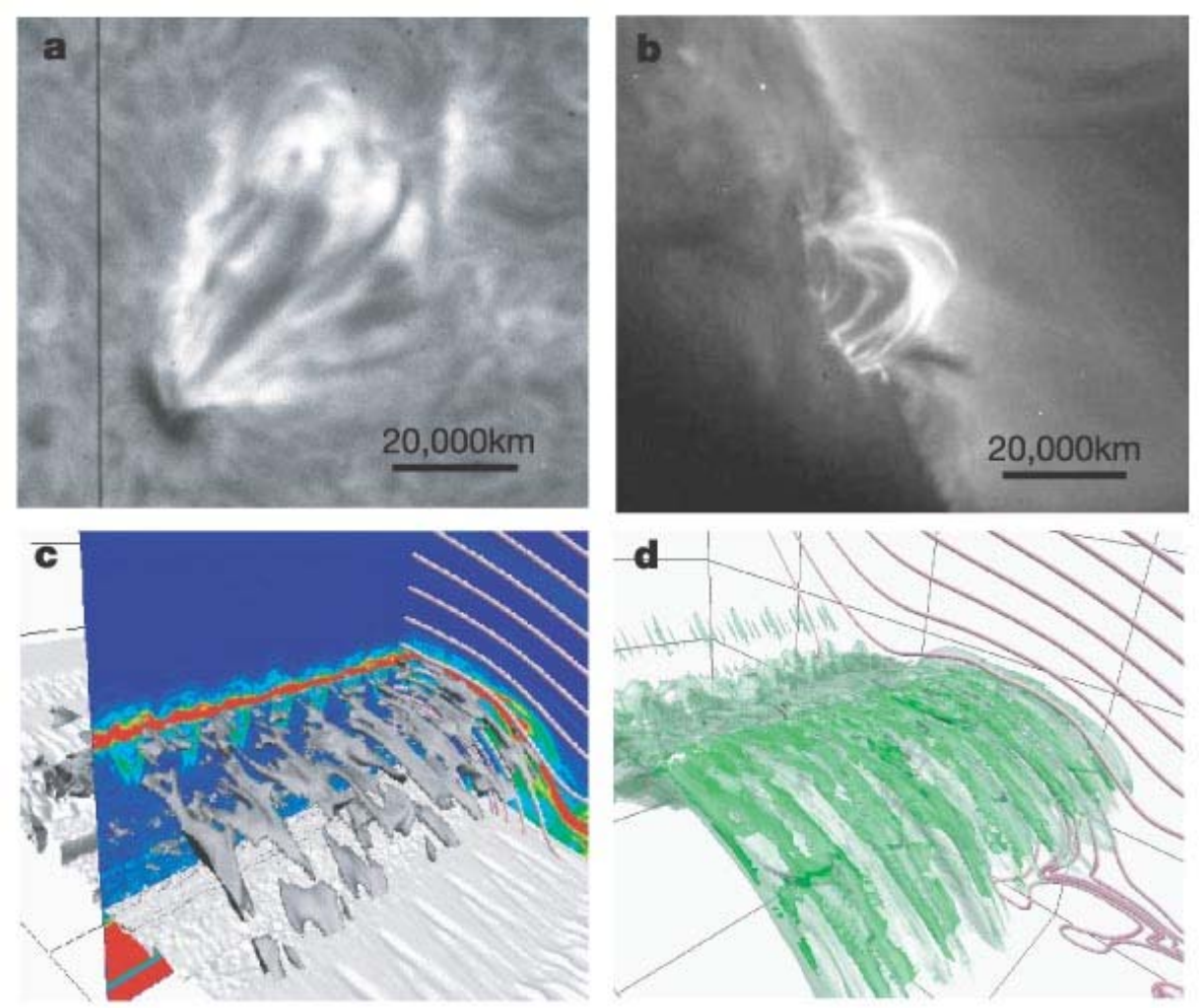

Isobe et al. (2005), Nature 434, 478, Ha-images observed at Hida observatory

However, there is a problem with short heating scale heights: Rayleigh-Taylor instability sets in at $s_h < L/3$ (Serio et al. 1981, Winebarger et al. 2003)

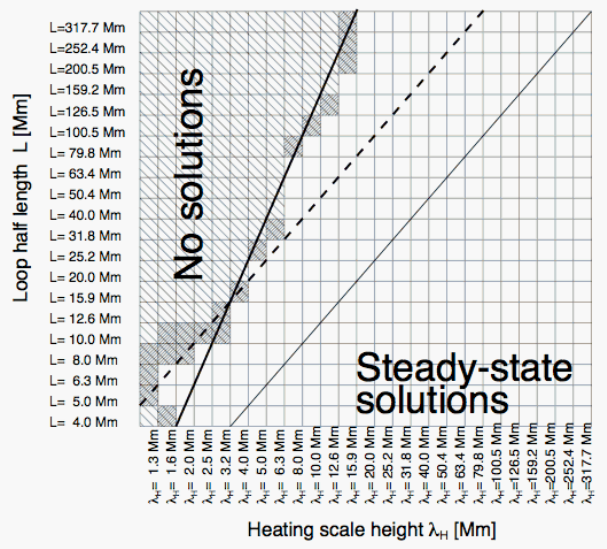

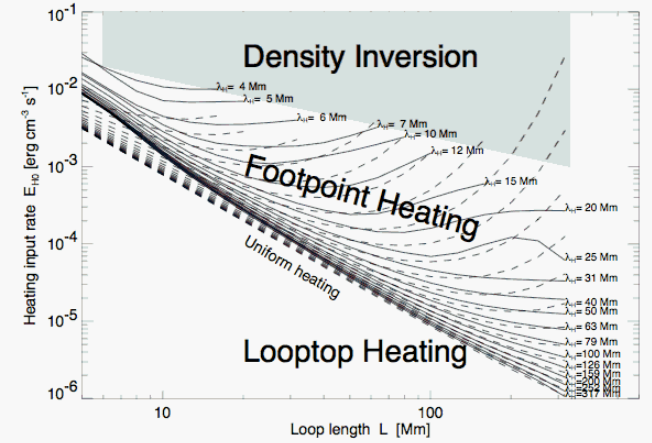

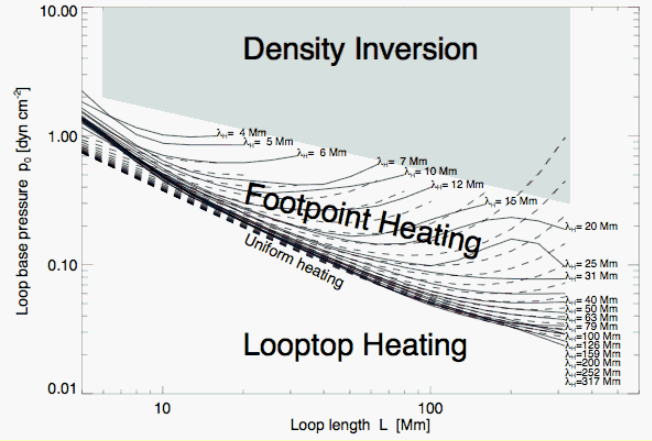

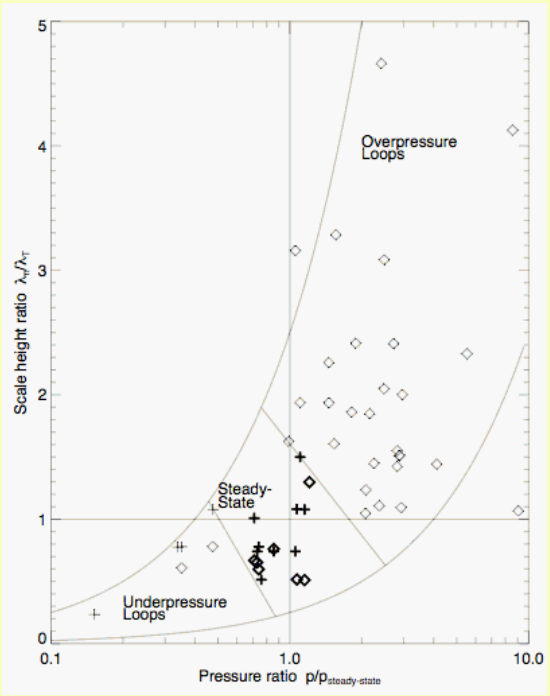

70% of the TRACE loops are found to be inconsistent with any stable hydrostatic solution

(Aschwanden, Schrijver & Alexander 2001)

Paradigm shift :

Equilibrium state $\Rightarrow$ Non-equilibrium state

Heating rate is NOT balancing loss rates (by thermal conduction and radiation)

RTV hydrostatic equilibrium solutions are not applicable most of the times.

Time-dependent MHD equations required

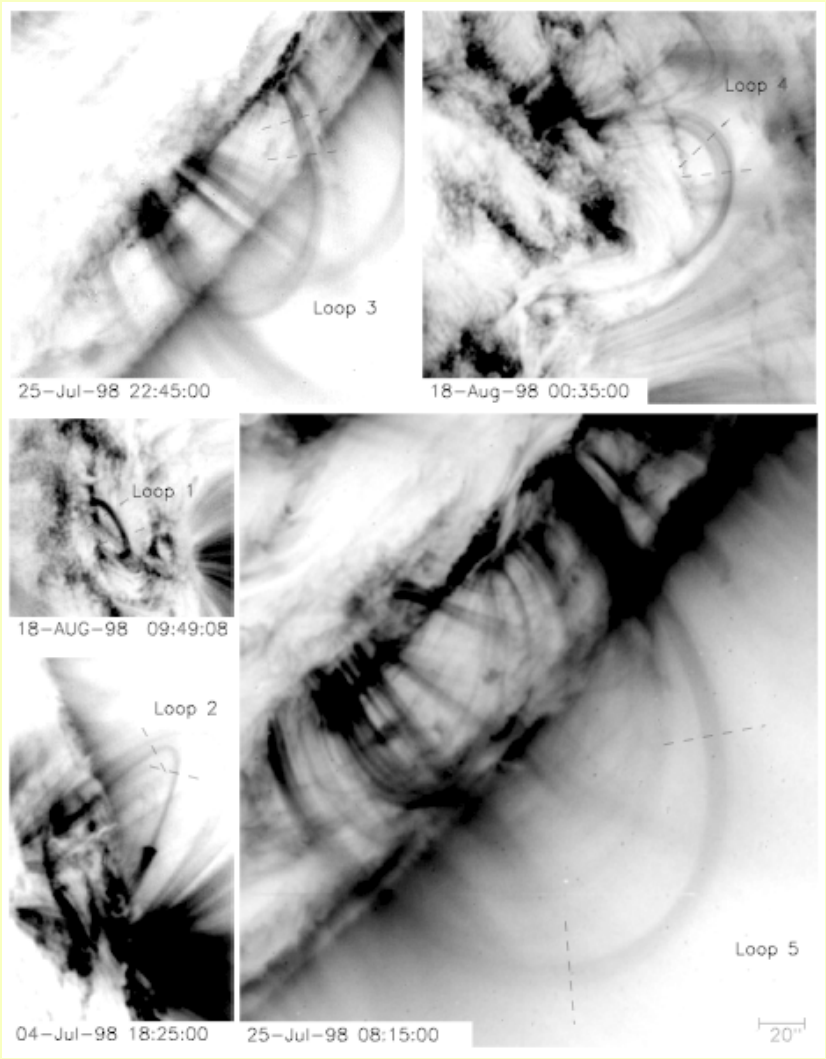

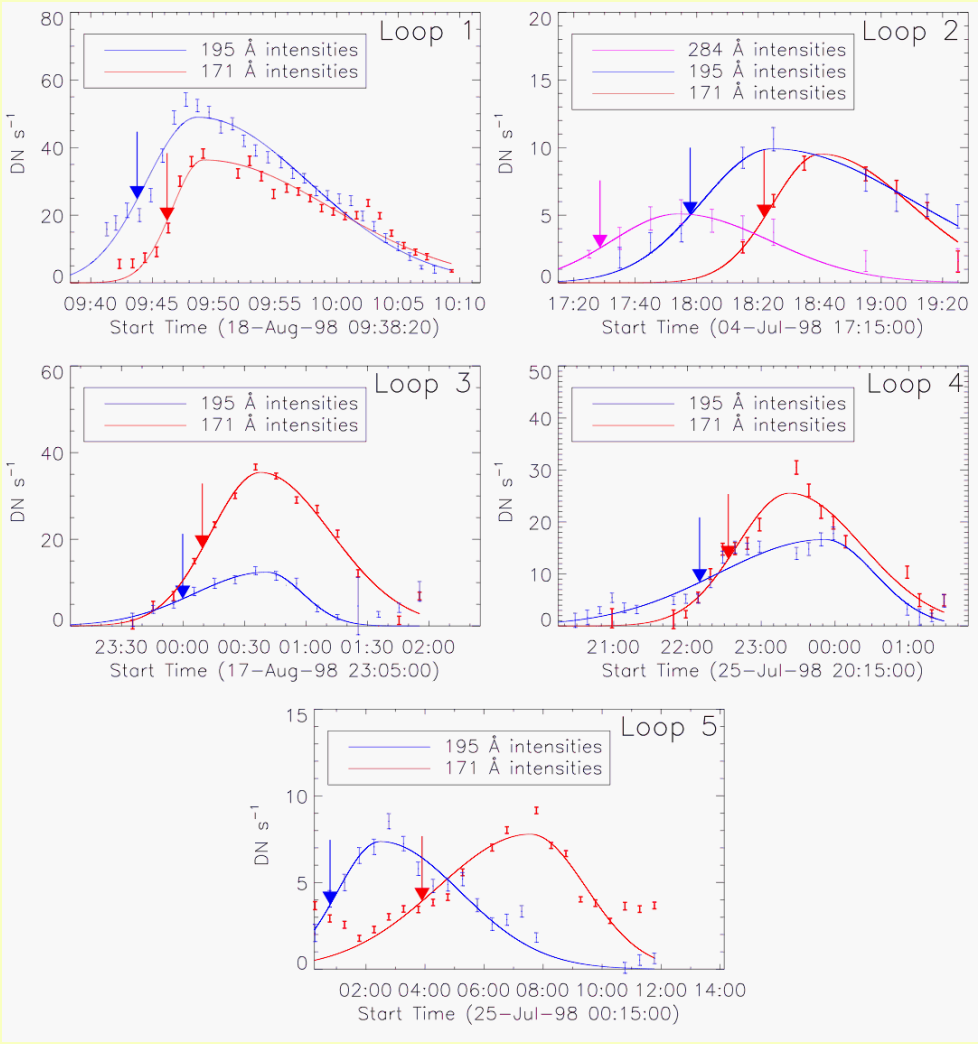

TRACE loops were observed to appear with a time delay between the 195 A (1.5 MK) and 171 A (1.0 MK) filters, which was interpreted in terms of a (non-equilibrium) cooling phase (Winebarger et al. 2003).

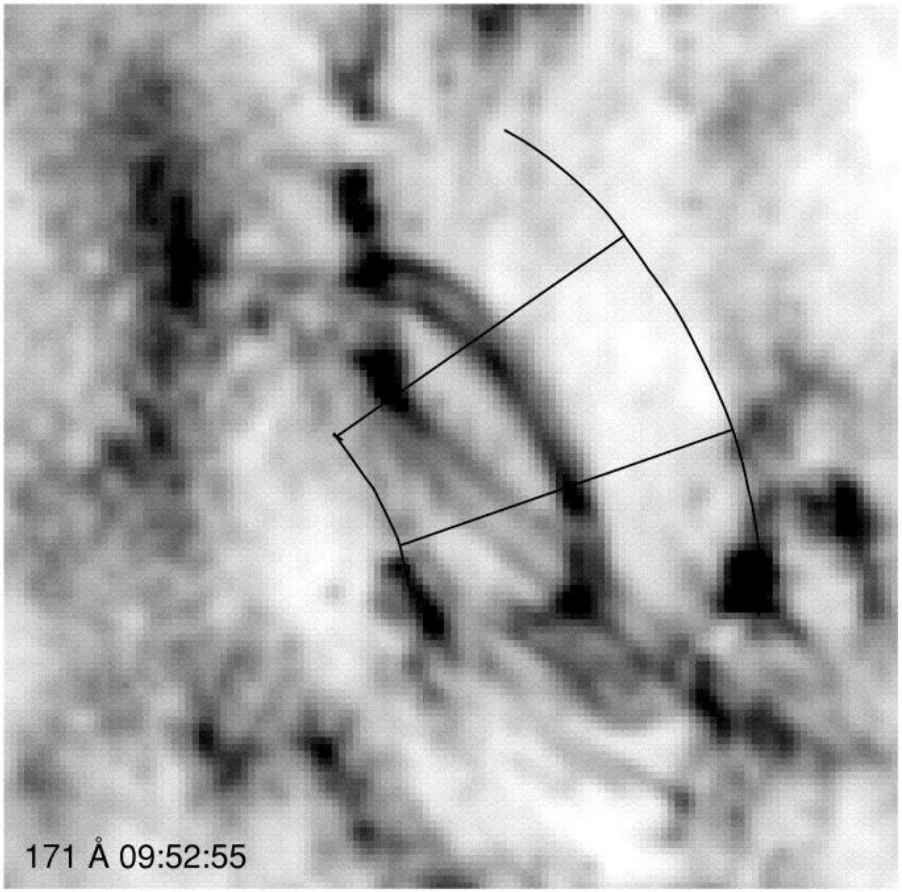

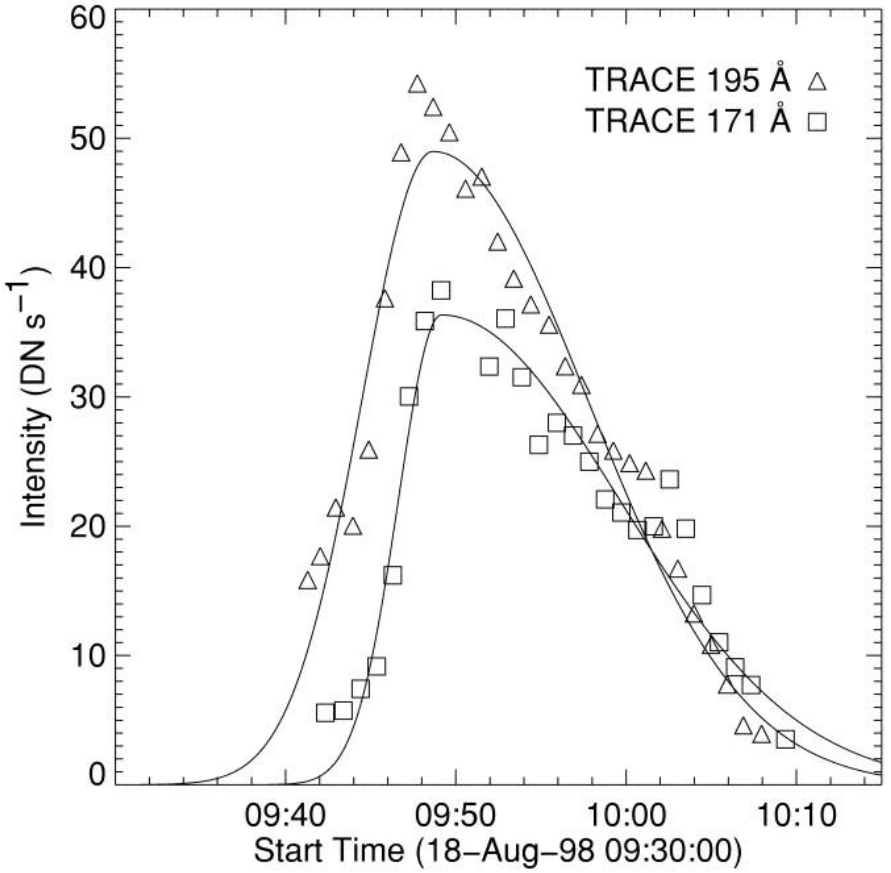

The cooling of a TRACE loop observed in 195 A and 171 A was modeled with hydrodynamic simulations, but the observed evolution could not be reproduced with an impulsively heated single loop (Warren, Winebarger & Mariska 2003).

Is this evidence for filamented multi-thread loops ?

Time-dependent hydrodynamic equations:

$$\rho \frac{De}{Dt} + p \nabla \mathbf{v} = E_H - E_R - \nabla F_C \ . \qquad (4.1.20)$$

The hydrodynamic equations (4.1.2−4) for coronal loops can be written more specifically, in one dimension, with loop coordinate s, by inserting the operator D/Dt explicitly, using $\rho = mn$, and the form (Eq. 4.1.20) of the energy equation,

---

$$\frac{\partial n}{\partial t} + \frac{\partial}{\partial s}(n\mathrm{v}) = 0 \ , \qquad (4.1.21)$$

$$mn \frac{\partial \mathrm{v}}{\partial t} + mn\mathrm{v} \frac{\partial \mathrm{v}}{\partial s} = -\frac{\partial p}{\partial s} + \frac{\partial p_{grav}}{\partial r}\left(\frac{\partial r}{\partial s}\right) \ , \qquad (4.1.22)$$

$$mn \frac{\partial e}{\partial t} + mn\mathrm{v} \frac{\partial e}{\partial s} + p \frac{\partial \mathrm{v}}{\partial s} = E_H - E_R - \frac{\partial F_C}{\partial s} \ . \qquad (4.1.23)$$

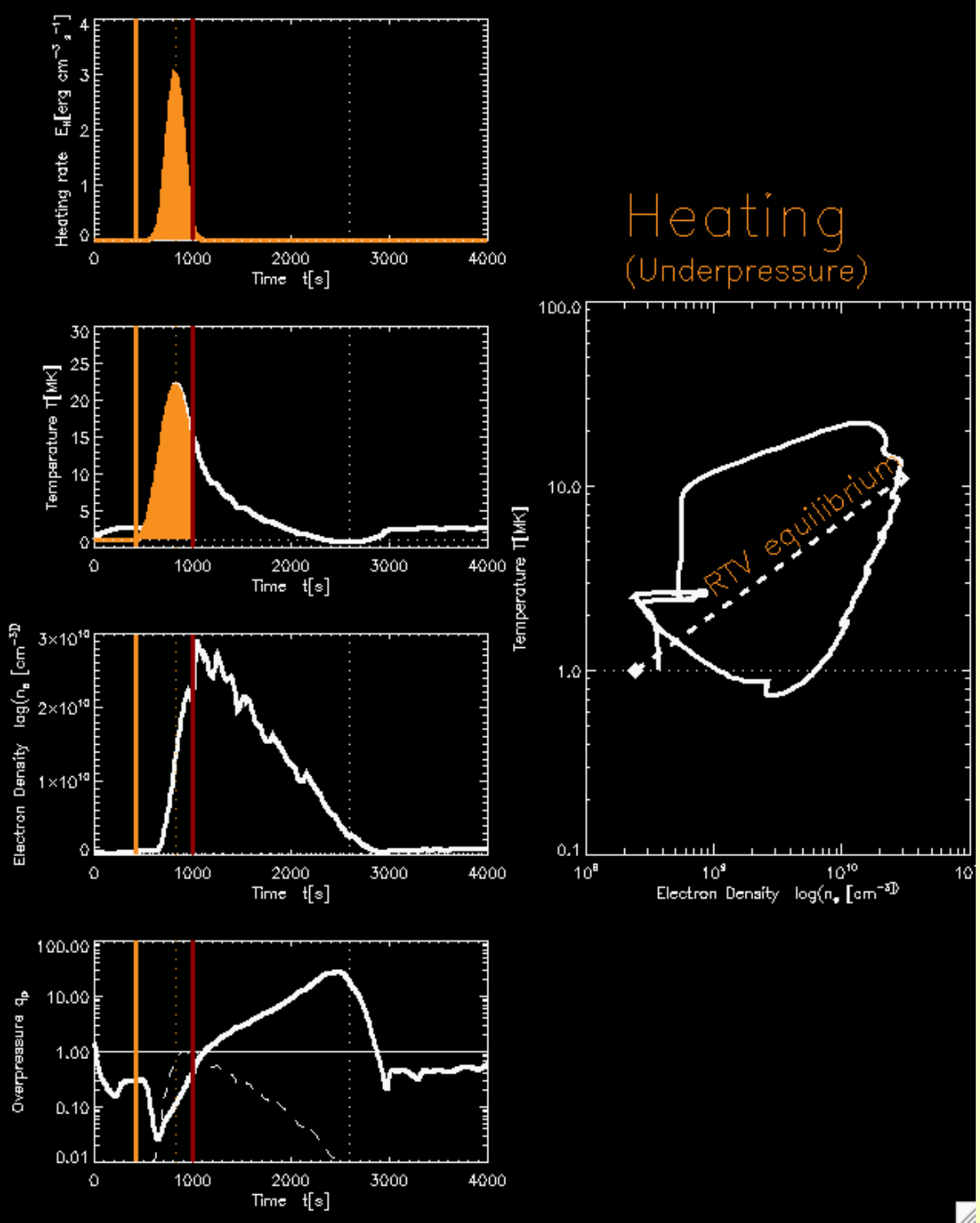

The temperature evolution T(t) of the heating phase can be analytically described from the evolution of the heating function (neglecting radiative loss)

$$E_H(s,t) - \frac{d}{ds}\left[\frac{2}{7}\kappa T(s)^{5/2}\frac{dT}{ds}\right] = \frac{2}{7}\kappa\frac{d^2T^{7/2}(s)}{ds^2}$$

$$E_{Hm} = E_H(t=t_m) \approx 2\kappa\frac{T_m^{7/2}}{L^2}$$

$$T(t<t_m) = \left[\frac{L^2}{2\kappa}E_H(t)\right]^{2/7}$$

Gaussian heating function

$$E_H(t) = E_{Hm}\exp\left(-\frac{(t-t_m)^2}{2\tau_{heat}^{\ 2}}\right)$$

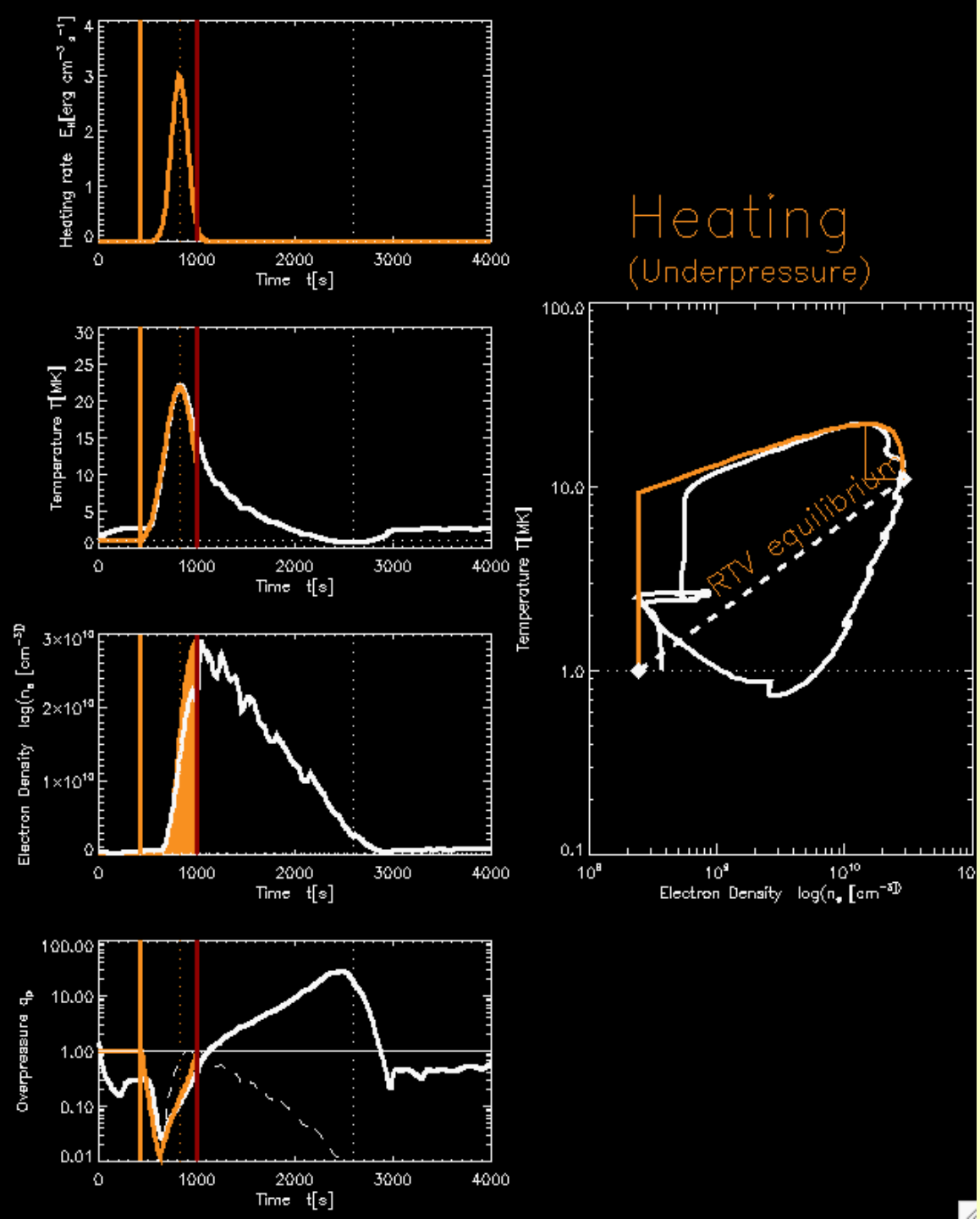

The electron density evolution n(t) of the heating phase can be analytically described with the Neupert effect: the density increases with the time integral of the evaporation rate (=heating rate)

$$n(t) \propto \int_0^t \left(\frac{E_H(t)}{E_{Hm}} \right) dt', t < t_p$$

$$n_p = n(t = t_p)$$

$$n_m = n(t = t_m) = n_p \frac{T_p}{T_m} = \frac{n_p}{2}$$

$$p \propto n_m T_m \approx n_p T_p$$

Pressure approximately constant near peak time

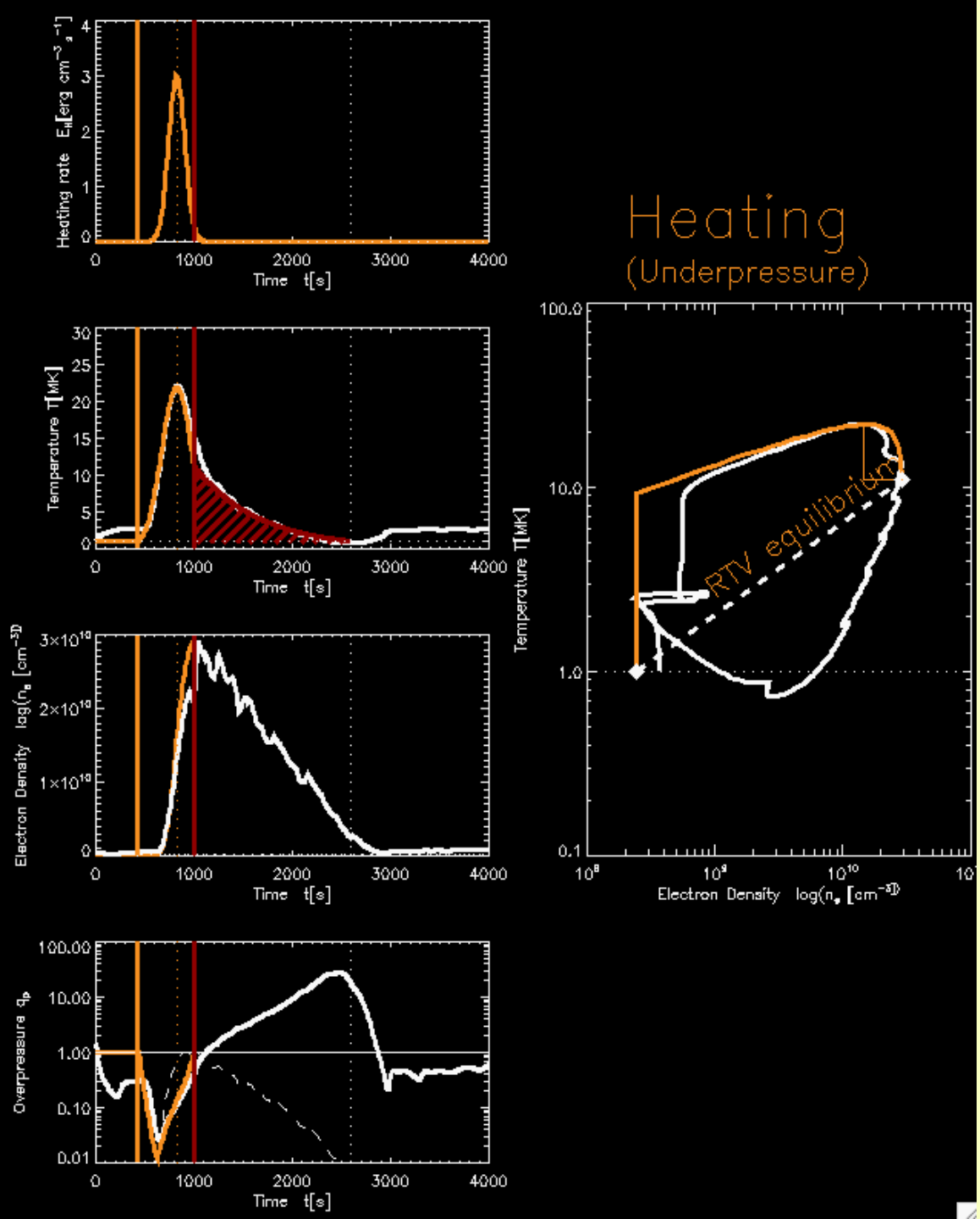

The temperature evolution T(t) in the cooling phase is Initially dominated by thermal conduction, and later by radiative loss (for low densities or low temperatures)

$$T(t) = T_p\left[1 + \frac{(t - t_p)}{\tau_{cool}}\right]^{-2/5}, t > t_p$$

$$\frac{3}{5}\frac{1}{\tau_{cool}} = \frac{2}{7}\frac{1}{\tau_{cond}} + \frac{3}{5}\frac{1}{\tau_{rad}},$$

$$\tau_{cond} = \frac{21}{5}\frac{n_p k_B L^2}{\kappa T^{5/2}},$$

$$\tau_{rad} = \frac{9 k_B T_p^{5/3}}{5 n_p \Lambda_0}.$$

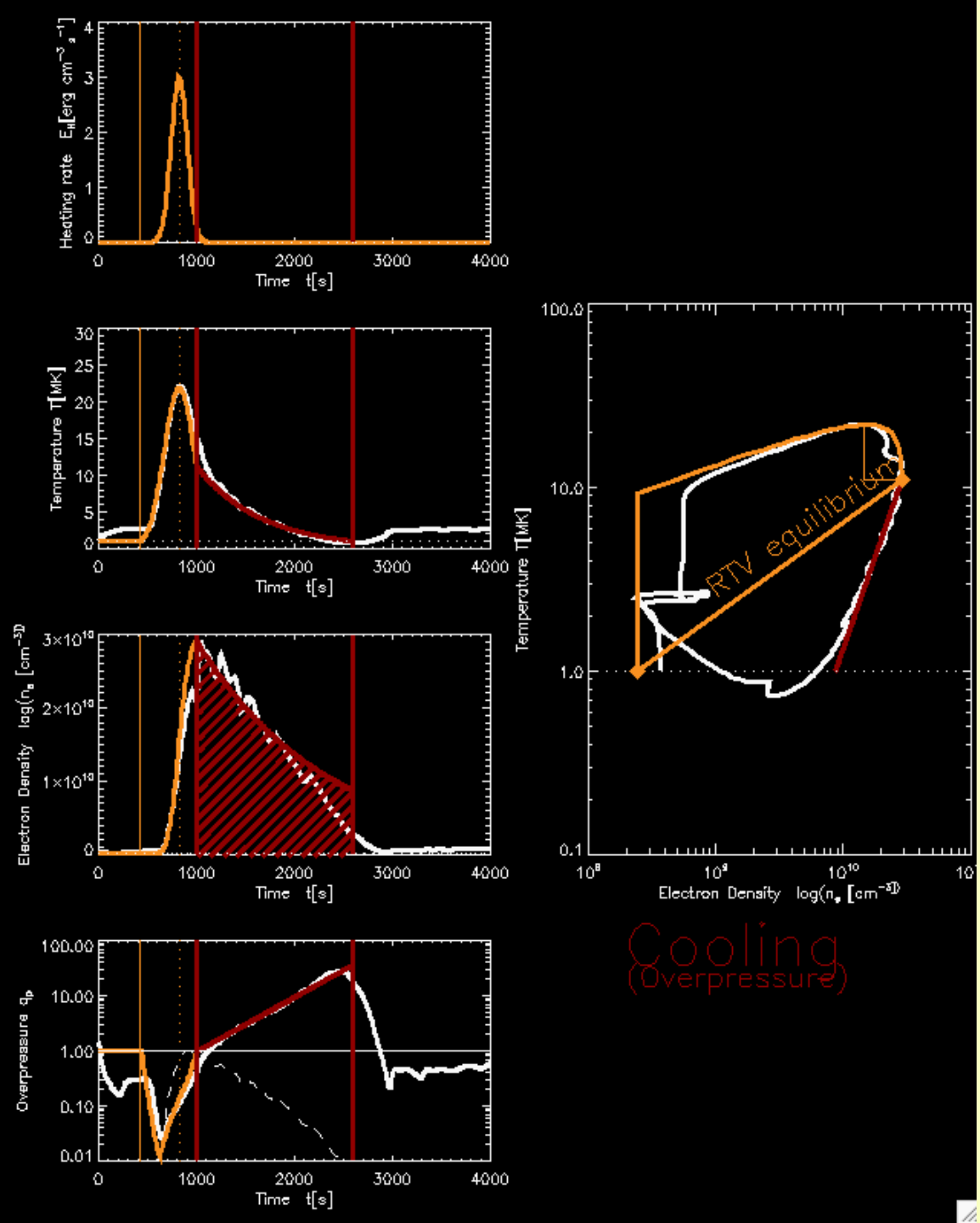

The electron density evolution n(t) in the cooling phase is related to the temperature evolution T(t) by a powerlaw function (Jakimiec relation)

$$\frac{n(t)}{n_p} \cong \left(\frac{T(t)}{T_p}\right)^2,$$

$$n(t) = n_p\left[\frac{T(t)}{T_p}\right]^{1/2}$$

$$= n_p\left[1 - \frac{(t-t_p)}{\tau_{cool}}\right]^{3/10}$$

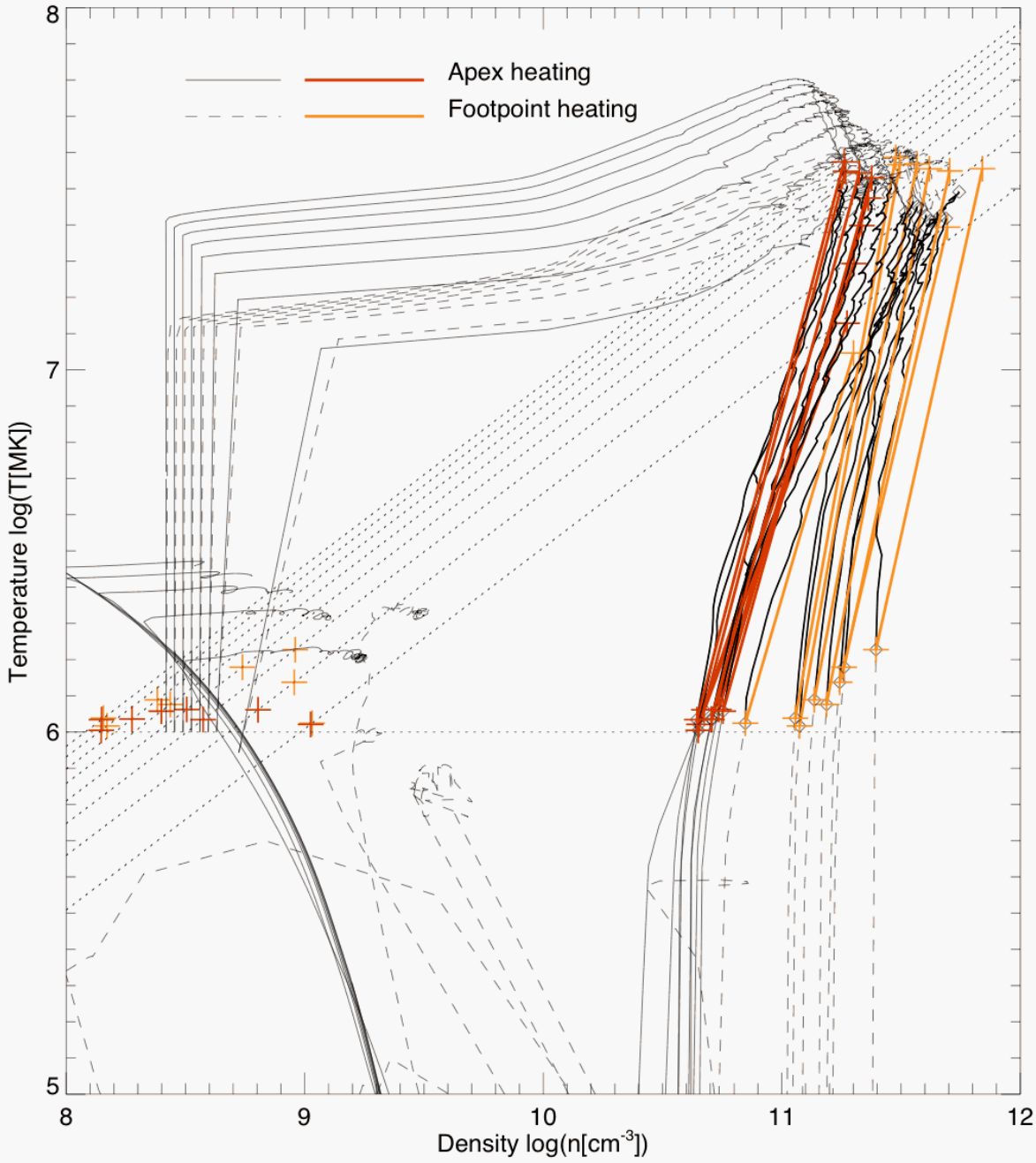

Hydrodynamic Simulations

(Tsiklauri et al.2004)

Cooling phase

$n(t) \sim T(t)^2$

(Jakimiec et al. 1992)

Analytical approximations for the hydrodynamic evolution of impulsively heated coronal loops

Now we have all parameter constants to express the evolution of the temperature profile $T(s=L,t)$ at the loop apex (Eqs. 24, 52),

$$T(s=L,t) = \begin{cases} T_m \left[\exp\left(-(t-t_m)^2/2\tau_{heat}^2\right)\right]^{2/7} & \text{for } t \le t_p \\ T_p \left[1-(t-t_p)/\tau_{cool}\right]^{3/5}] & \text{for } t > t_p \end{cases} , \quad (57)$$

and the evolution of the density profile $n(s=L,t)$ at the loop apex (Eqs. 33, 56),

$$n(s=L,t) = \begin{cases} n_p \ \exp\left(-(t-t_p)^2/2\tau_{evap}^2\right) & \text{for } t \le t_p \\ n_p \ \left[1-(t-t_p)/\tau_{cool}\right]^{3/10} & \text{for } t > t_p \end{cases} . \quad (58)$$

The spatial profiles can be approximated with equilibrium solutions (which may be less accurate for short heating rates). The spatial loop profile is then according to the solution given in Eq. (22) and the loop apex evolution $T(s=L,t)$ given in Eq. (57),

$$T(s,t) = T(s=L,t) \left[\left(\frac{s}{L}\right) + 2q_H \left(\frac{s_H}{L}\right)^2 \left(1 - \exp\left(-\frac{s}{s_H}\right) - \left(\frac{s}{L}\right)\left[1-\exp\left(-\frac{L}{s_H}\right)\right]\right)\right]^{2/7} . \quad (59)$$

The pressure or density scale height λ_T (Eq. 37) of hydrostatic loops is a function of the temperature, for which we can use approximately the expression for the apex temperature $T(s=L,t)$, yielding (with Eq. 38)

$$n(s,t) = n(s=L,t) \ \left(\frac{T(s=L,t)}{T(s,t)}\right) \ \exp\left(-\frac{h(s)-H}{\lambda_p(T[s=L,t])}\right) . \quad (60)$$

where $H = h(s=L)$ is the height of the loop apex. This set of analytical equations (57-60) provides then an complete approximation to the spatio-temporal evolution of loop temperatures $T(s,t)$ and loop densities $n(s,t)$. The validity range of this analytical code is limited to loop apex temperatures in the coronal range of $T_m \gtrsim 1.0$ MK.

Aschwanden & Tsiklauri (2008)

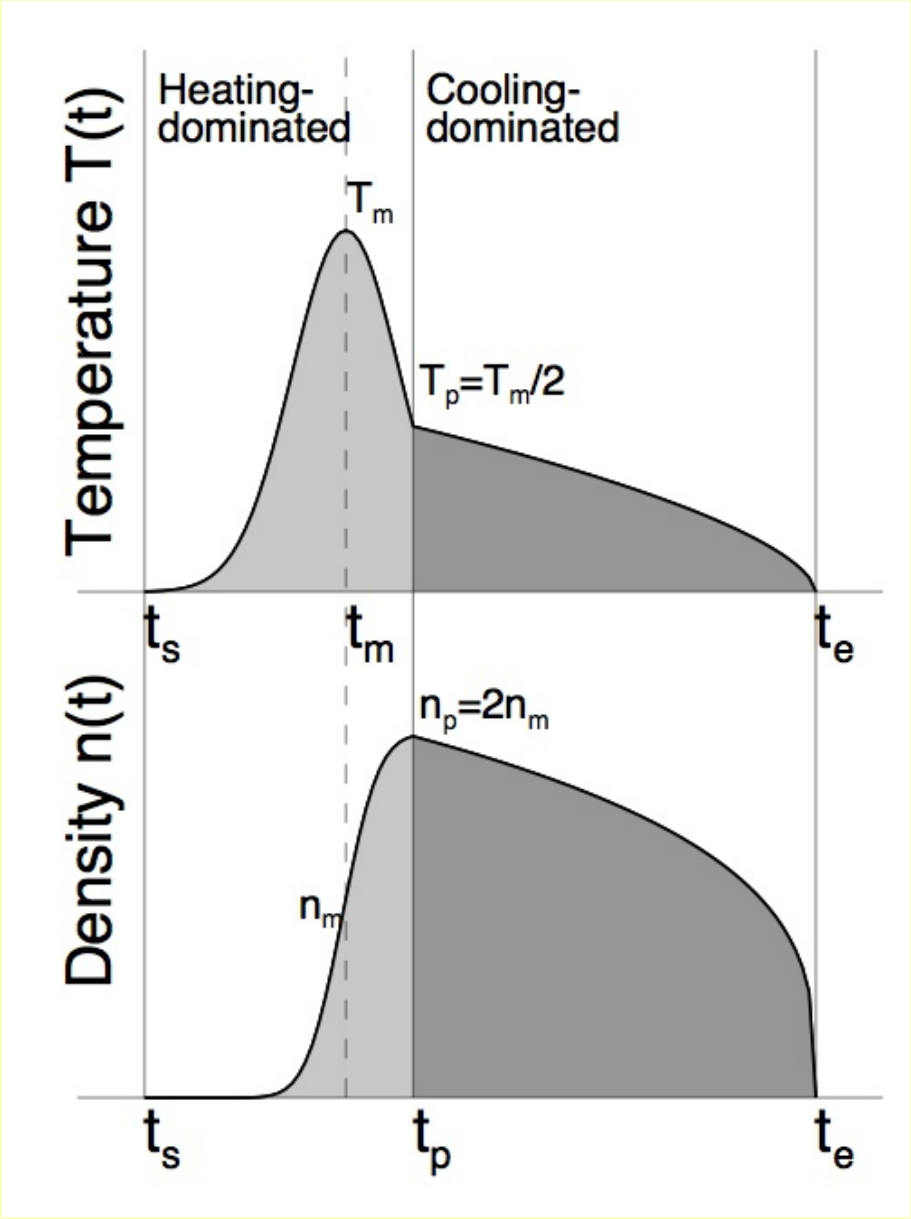

Analytical approximation

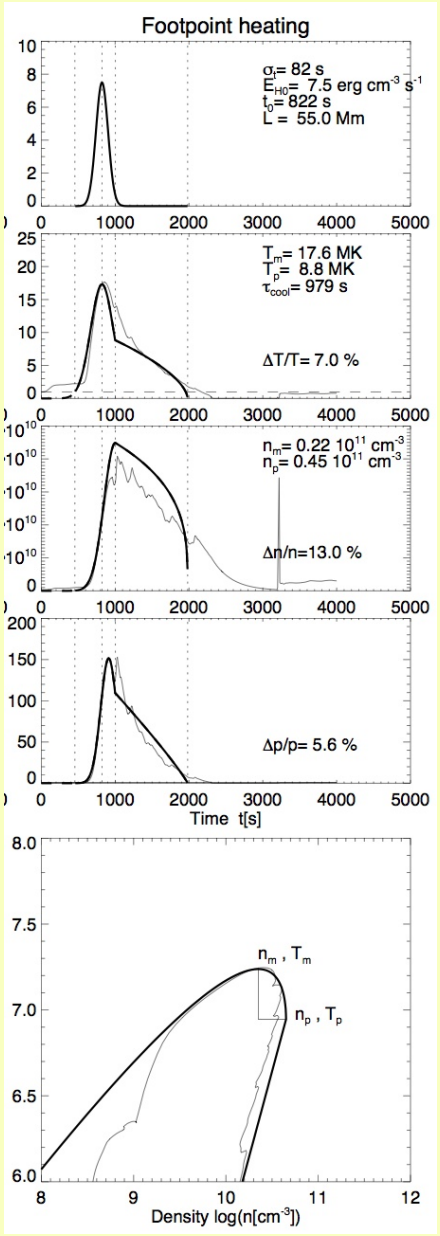

$E_H(t)$

$T(t)$

$n_e(t)$

$p(t)$

$T(n_e)$

Comparison with numerical simulation

Forward modeling of light curves in multiple wavelengths

Input parameters: Heating function H_0, t_m, τ_{heat}, s_H
Loop geometry L, w_L, p_{div}, θ

Heating function:

$$E_H(s,t) = H_0 \exp\left(-\frac{(t-t_m)^2}{2\tau_{heat}^2}\right) \exp\left(-\frac{s}{s_H}\right) \begin{cases} s_H > 0 & \text{for footpoint heating} \\ s_H = \infty & \text{for uniform heating} \\ s_H < 0 & \text{for apex heating} \end{cases}$$

Loop cross-section:

$$w(s) = w_L * \sin\left(\frac{\pi}{2}\frac{s}{L}\right)^{p_{div}}$$

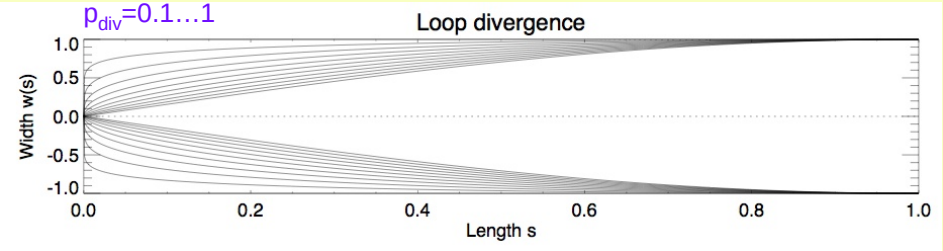

Emission measure:

$$\frac{dEM(T[s],t)}{dT} = n_e^2(s[T],t) * w(s)^2 * \frac{ds(T)}{dT}$$

Flux observed with instrument response function R(T):

$$F_{instr}(t) = \int \frac{dEM(T,t)}{dT} * R_{instr}(T) * dT$$

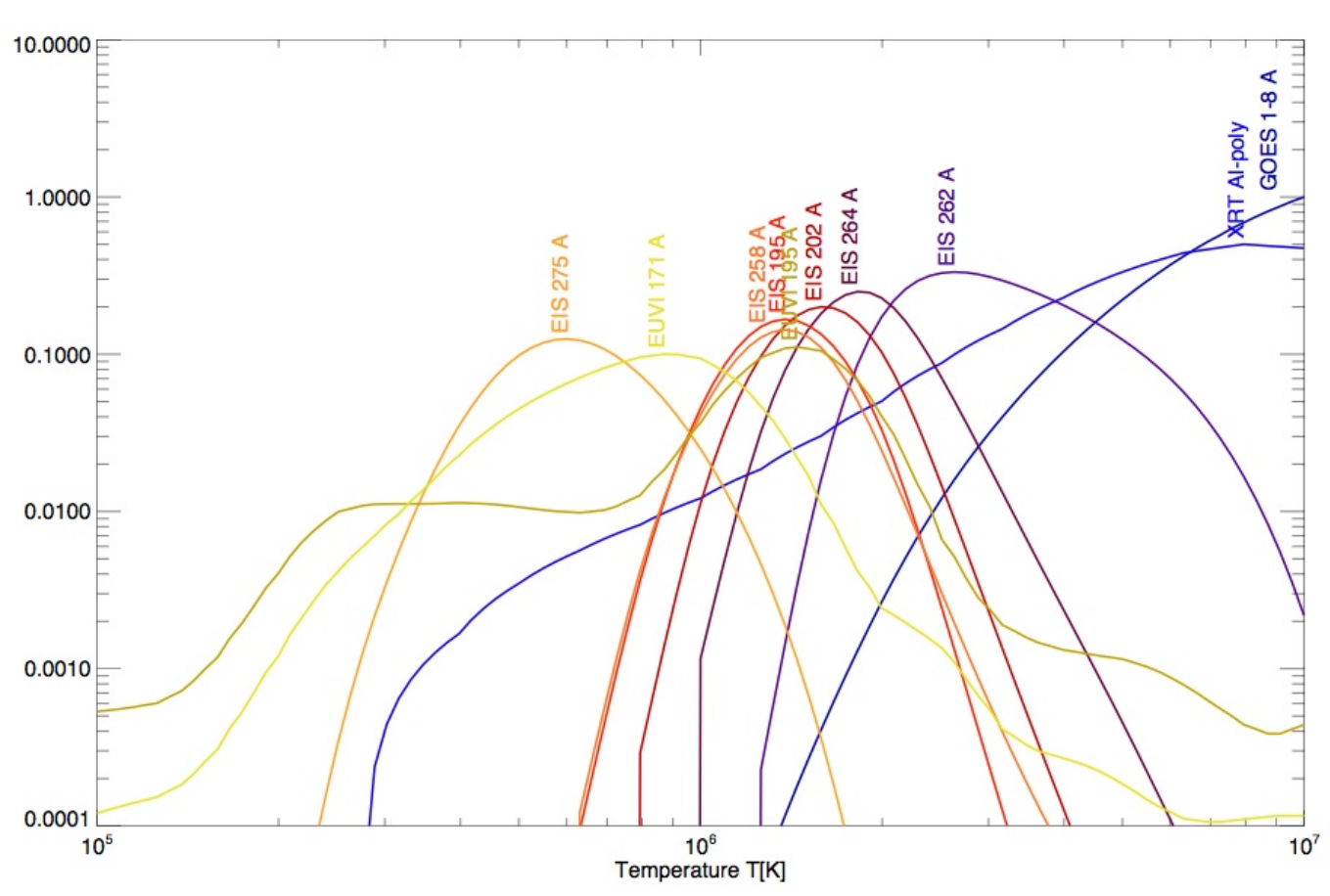

Response functions of EUVI, Hinode/EIS, XRT, & GOES: R(T)

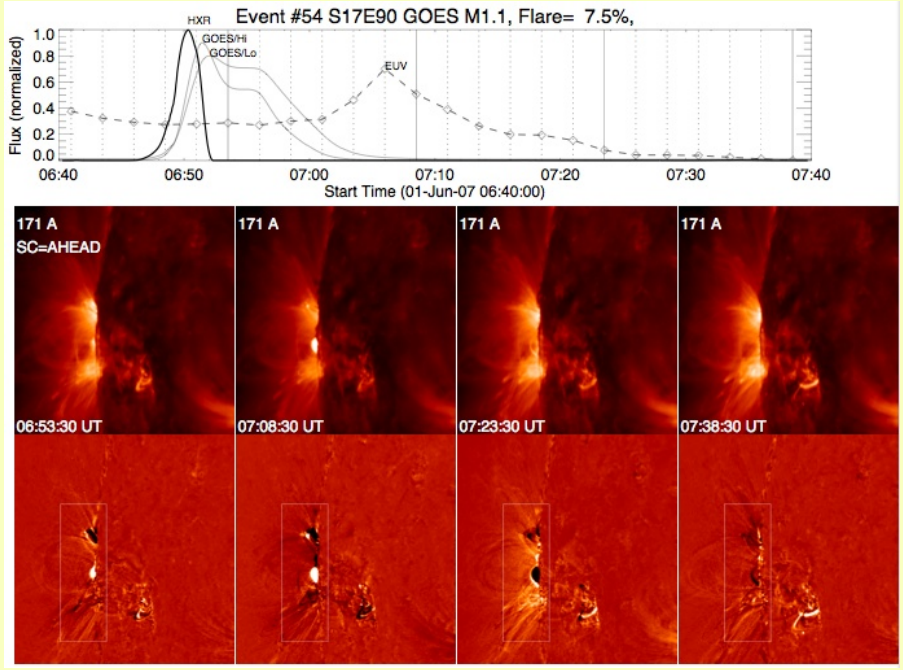

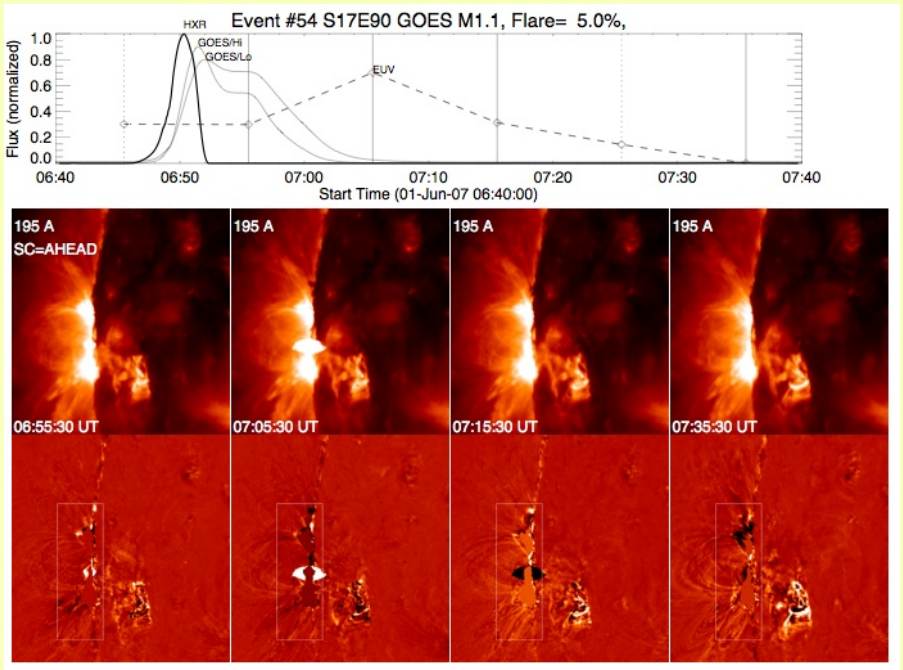

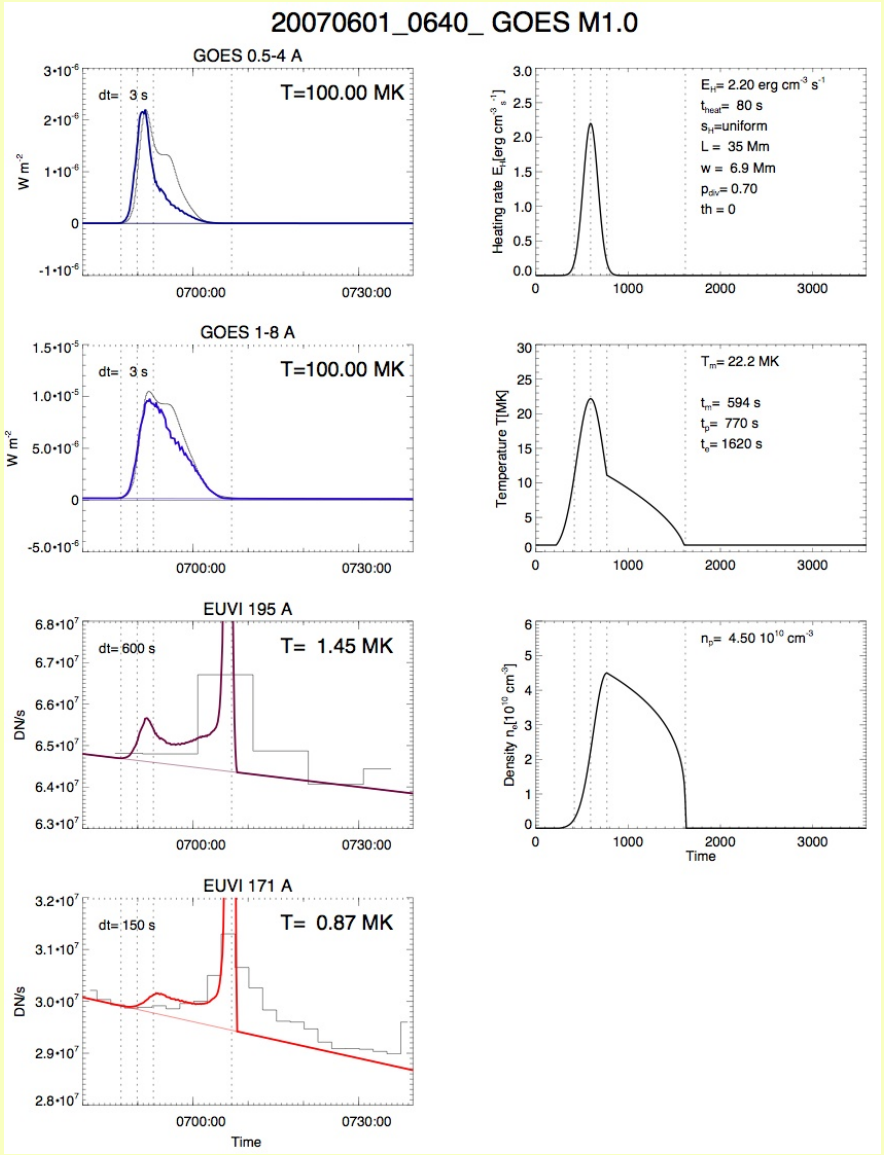

Max. Temp (T_m=22.2 MK) constrained by GOES
EUVI peaks 15 min later than SXR
Loop length constrained by observed geometry and cooling time of ~15 min ($\tau_{cond} \propto L^2 n_e T^{-5/2}$)

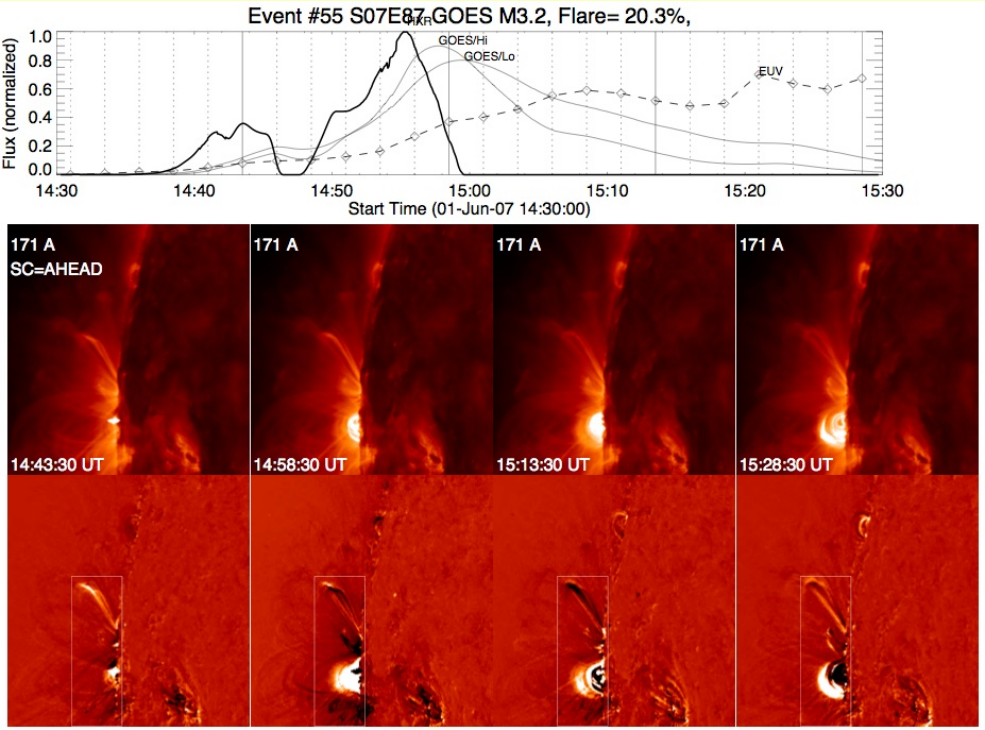

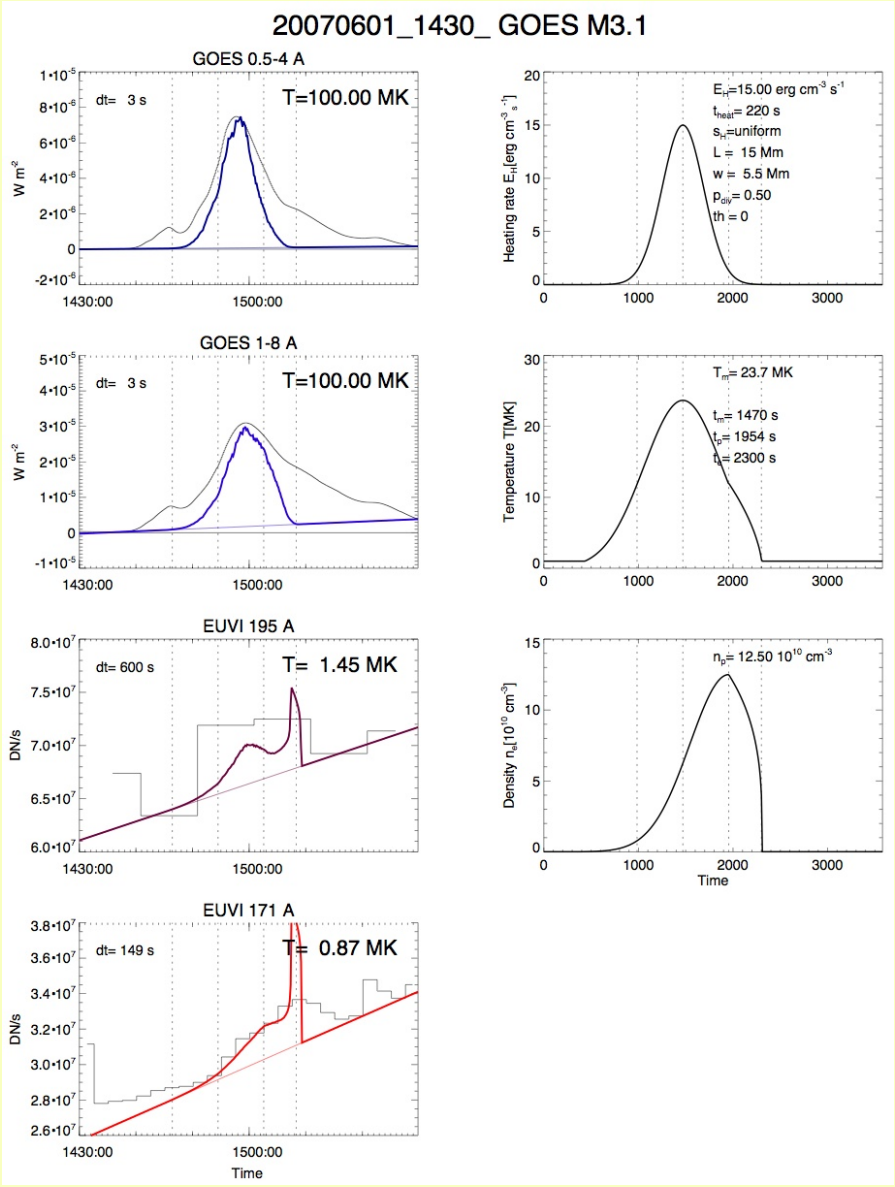

Loop length L=15 Mm constrained by stereoscopic measurement and cooling time

EUV peaks ~15 min after SXR

Maximum temperature T=23.7 MK constrained by GOES

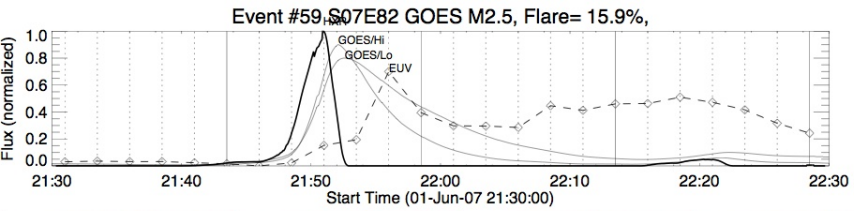

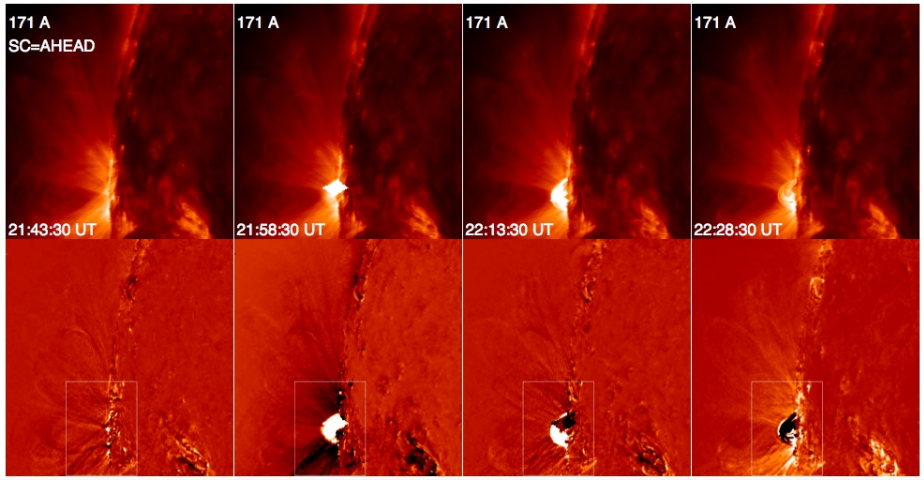

Loop half length L=15 Mm constrained
by observed geometry and EUV peak time

EUV peaks ~6 min after SXR

Max. temperature T=25.7 MK constrained
by GOES

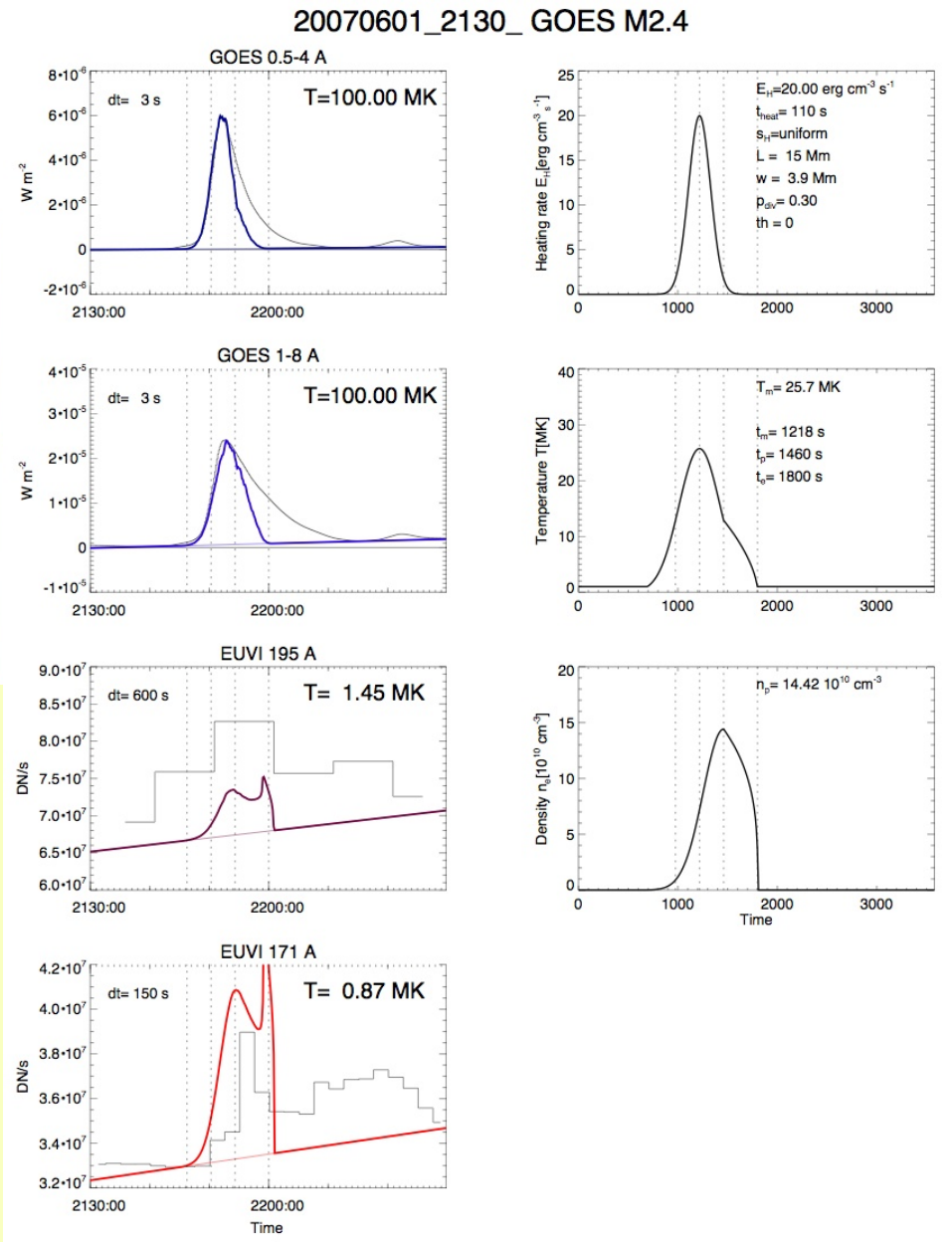

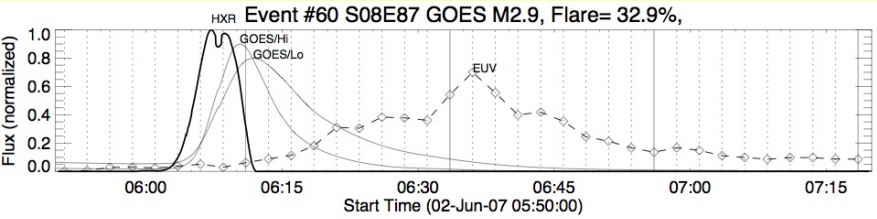

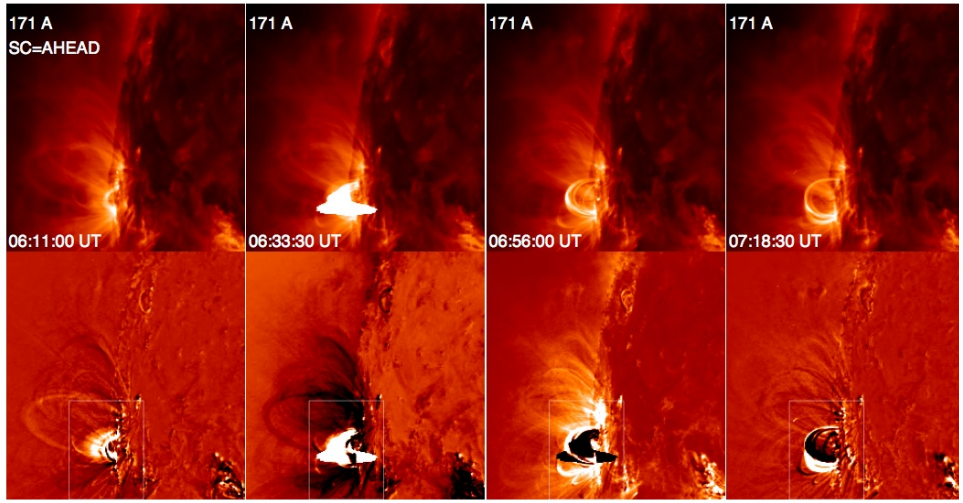

Loop half length L=65 Mm constrained by observed geometry and EUV peak time

EUV peaks ~30 min after SXR

Max. temperature T=28.3 MK constrained by GOES

Combined loop width w=6.4 Mm contains multiple loops

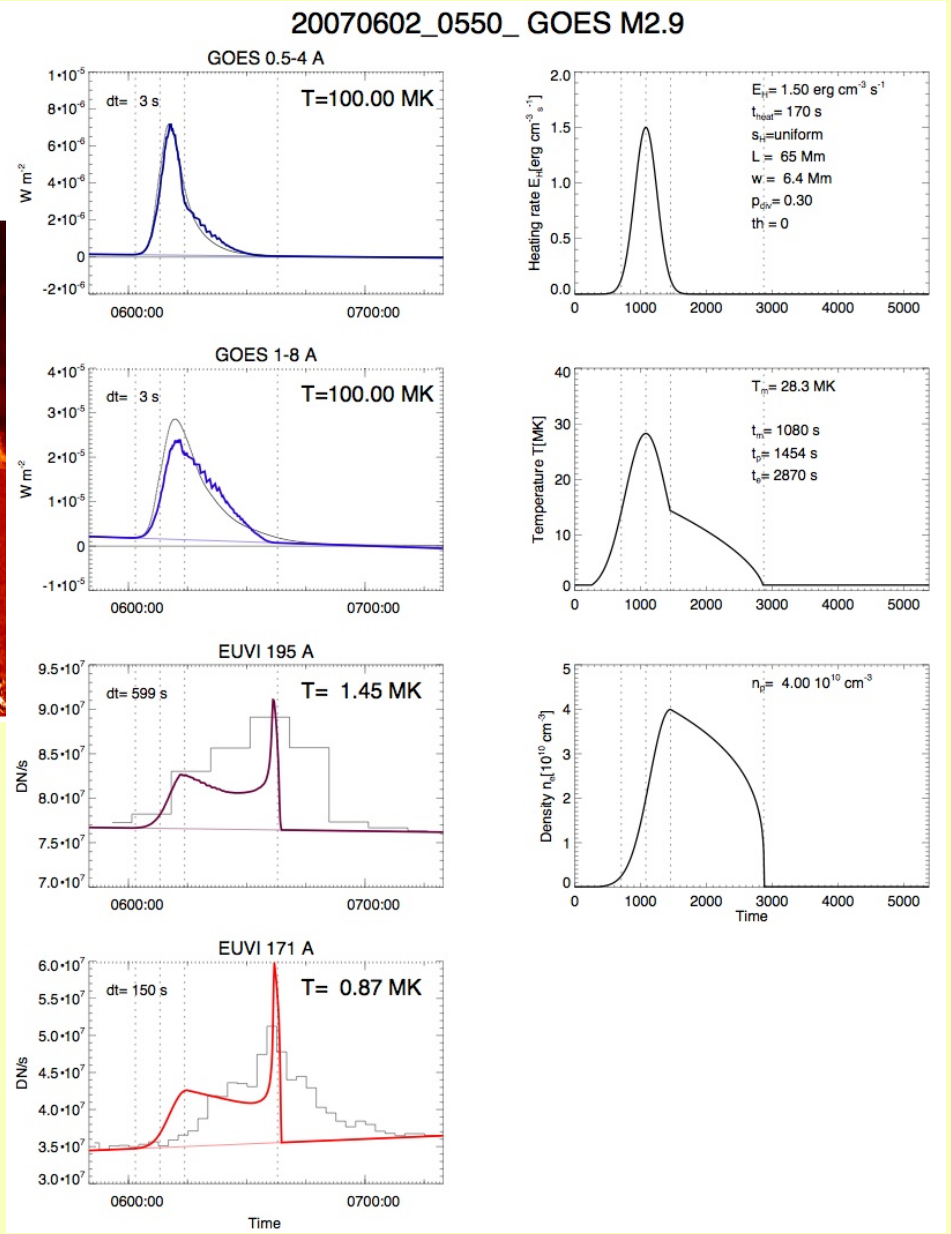

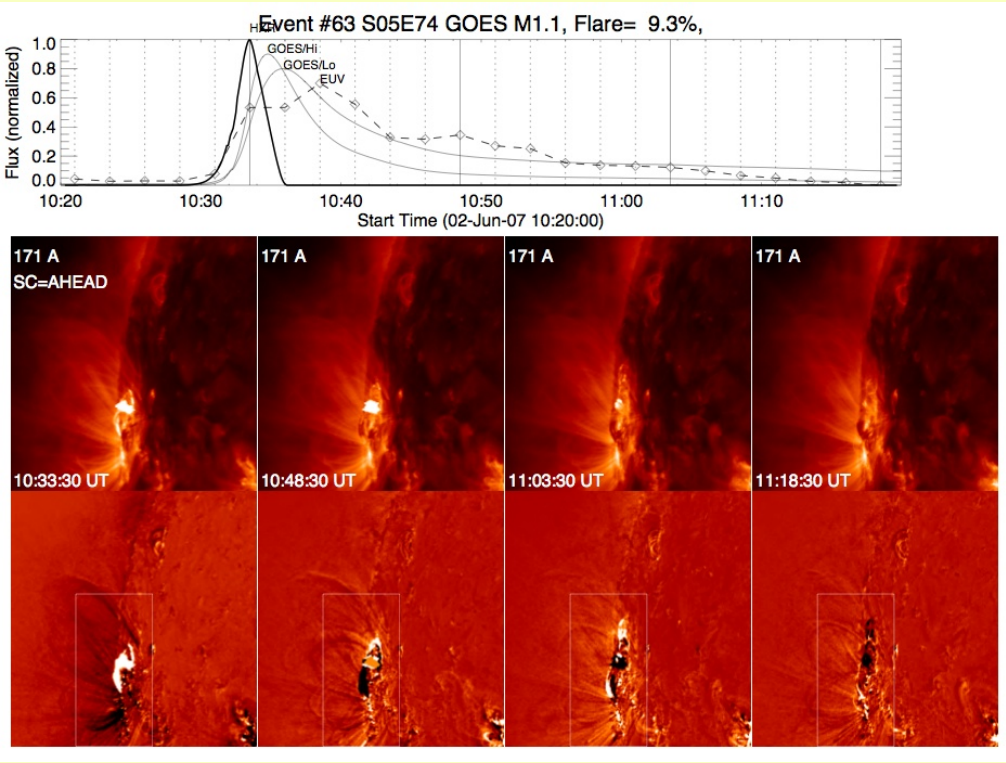

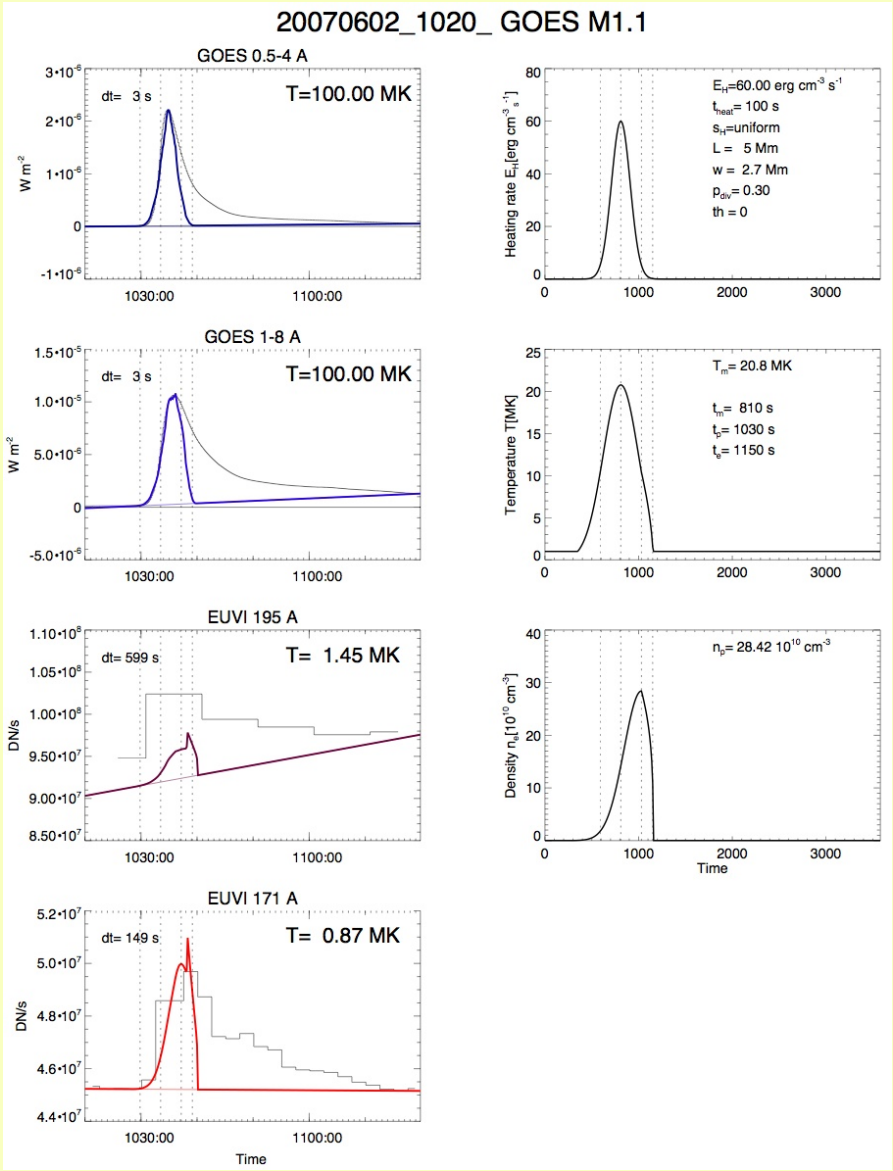

Very mall loop half length L=5 Mm

EUV peaks ~4 min after SXR

Max. temperature T=20.8 MK constrained by GOES

Loop width w=2.7 Mm (near resolution)

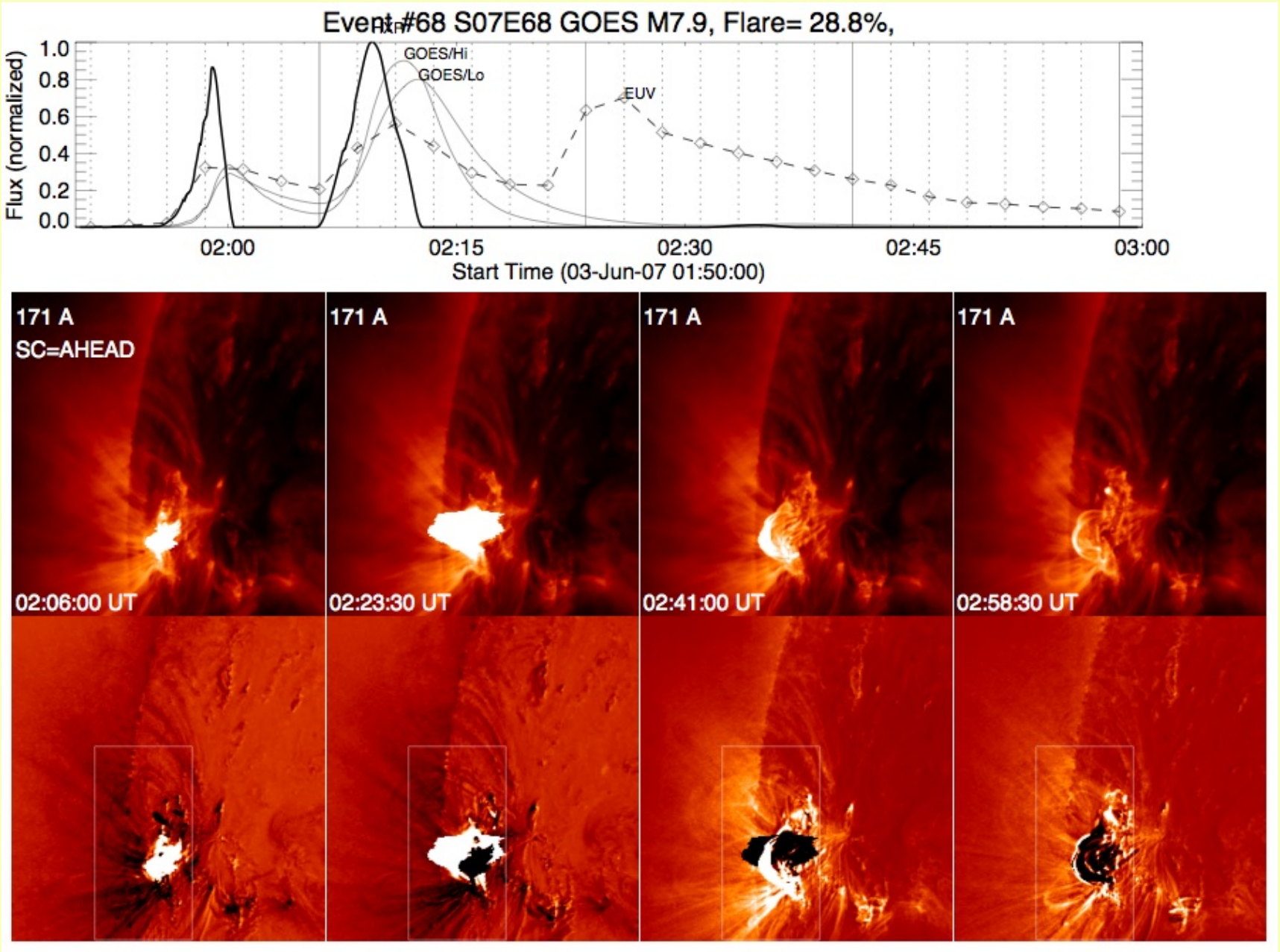

Two subsequent flares within 15 min

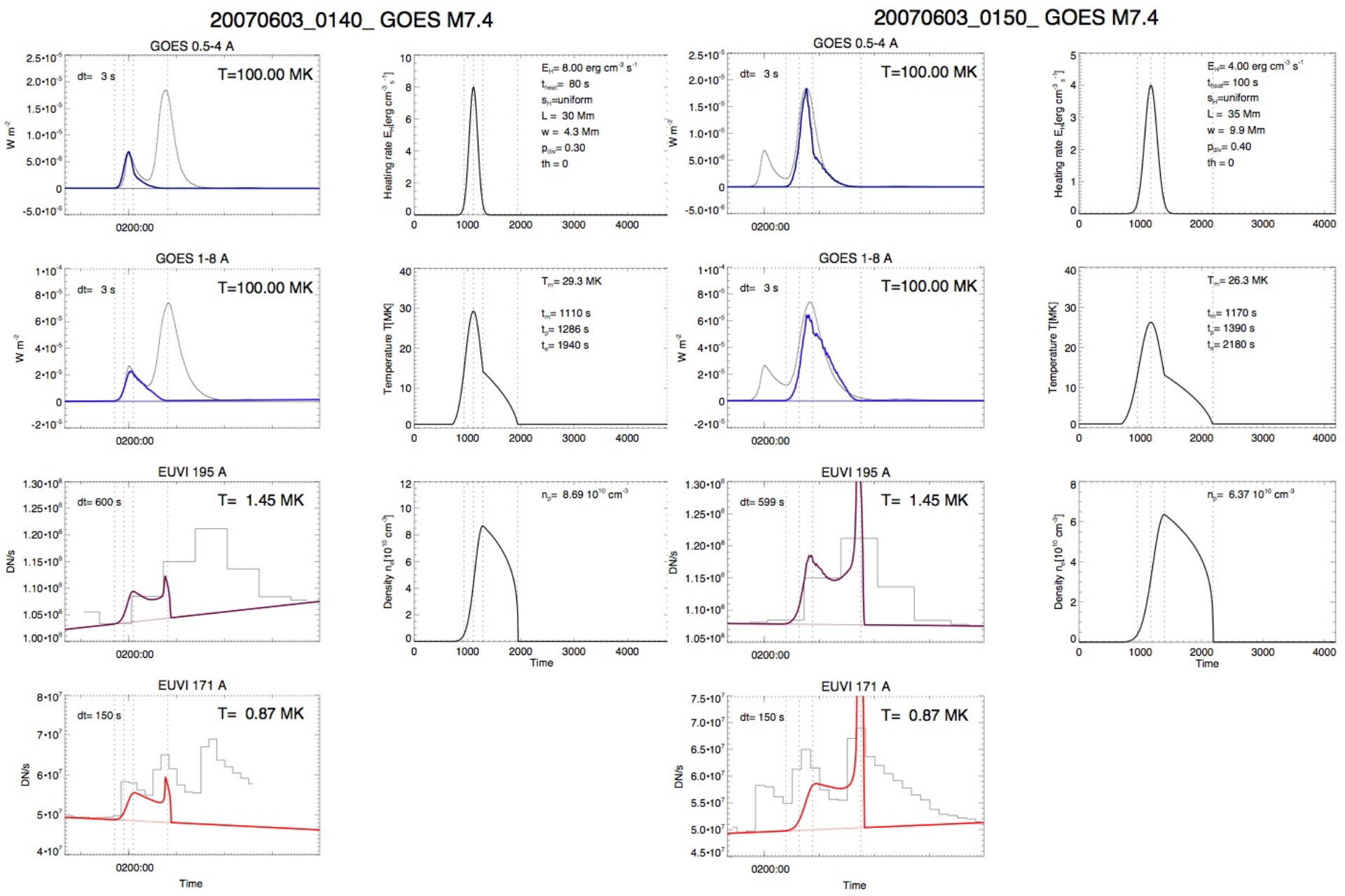

Two subsequent flares produce two EUV peaks in 171 A, with delays of 10-15 min

A GOES-class B1 flare observed with Hinode/EIS, XRT, and STEREO/EUVI

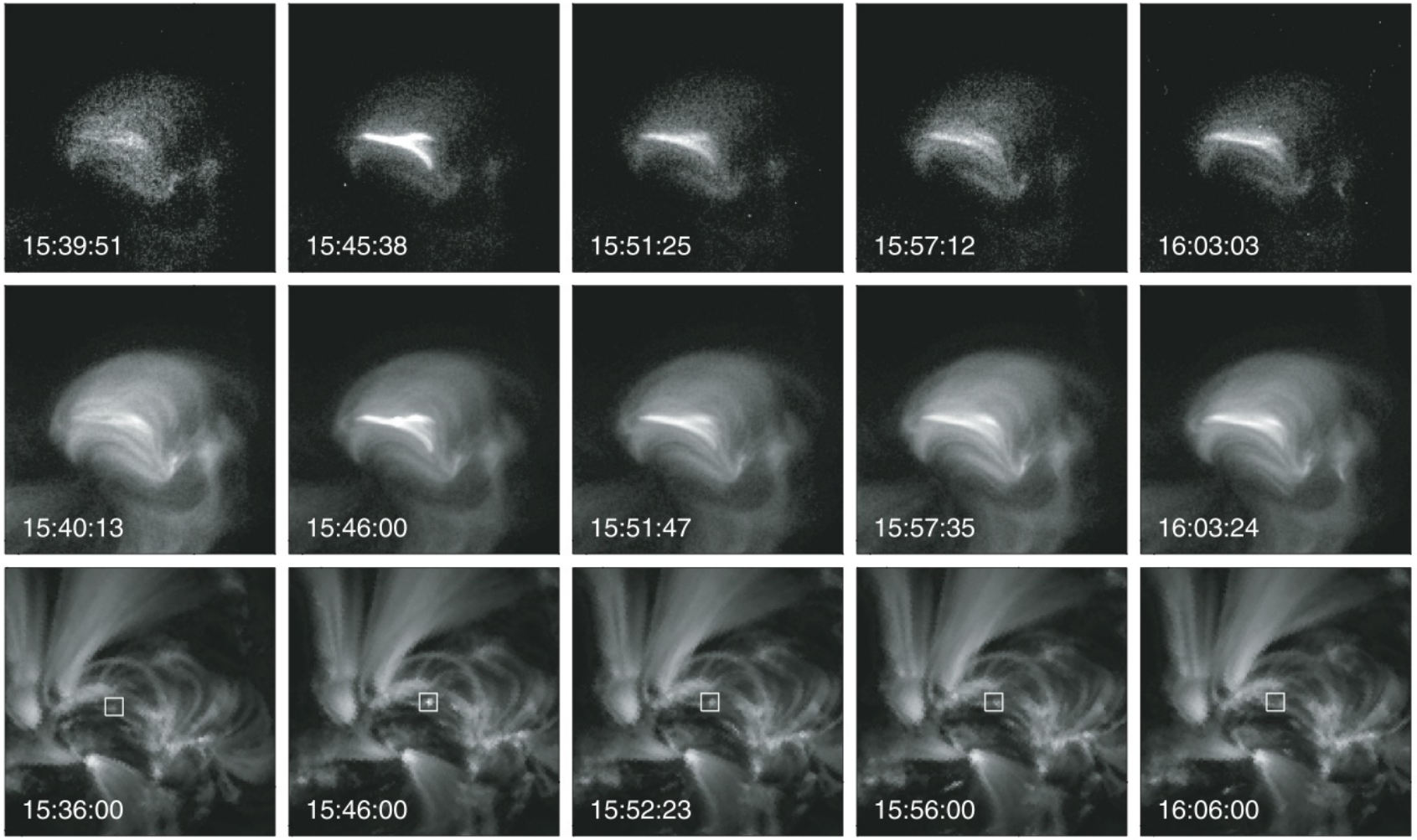

Fig. 4. XRT (Al-poly/Open and Al-poly/Al-thick) and STEREO B EUVI 171 Å images for the B flare observed on 2007 February 1 near 15:45. The spatial position of the footpoint spectra shown in figure 5 is indicated by the box. A movie is provided as on-line material.*

Warren et al. (2007), PASJ 59, S675

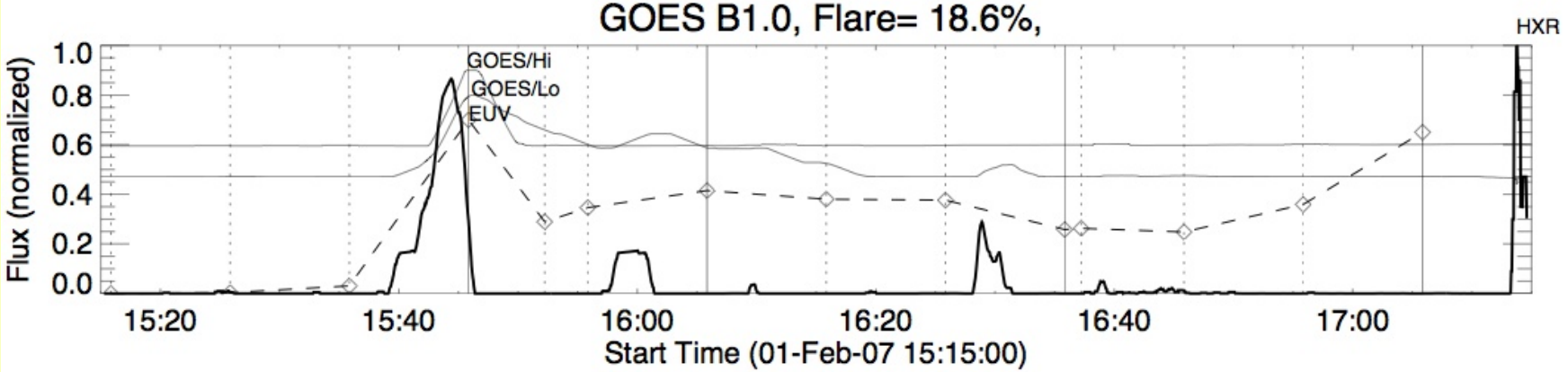
GOES B1.0, Flare= 18.6%,
HXR
GOES/Hi
GOES/Lo
EUV
Flux (normalized)
1.0
0.8
0.6
0.4
0.2
0.0
15:20
15:40
16:00
16:20
16:40
17:00
Start Time (01-Feb-07 15:15:00)

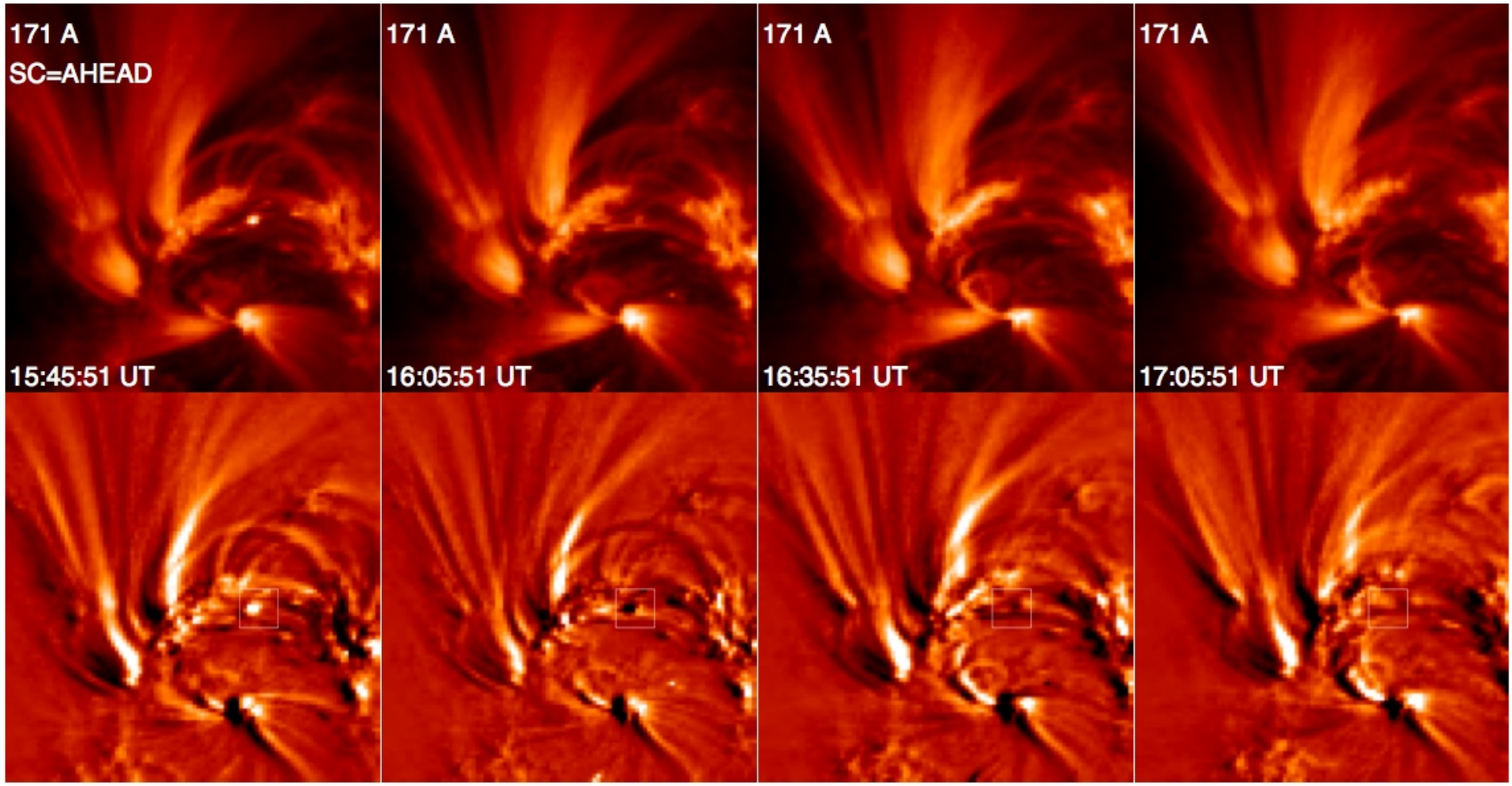
171 A
SC=AHEAD
15:45:51 UT
171 A
16:05:51 UT
171 A
16:35:51 UT
171 A
17:05:51 UT

During the brightening, the loop apex is observed with XRT and one loop footpoint (moss region) is observed with EUVI

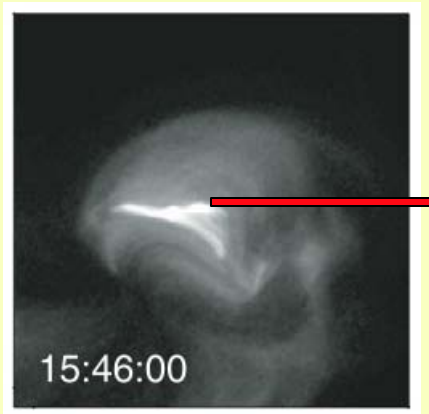

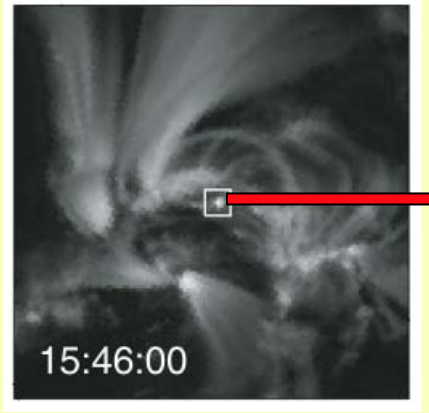

Loop apex
XRT T~8 MK

Footpoint
EUV T~1.0 MK

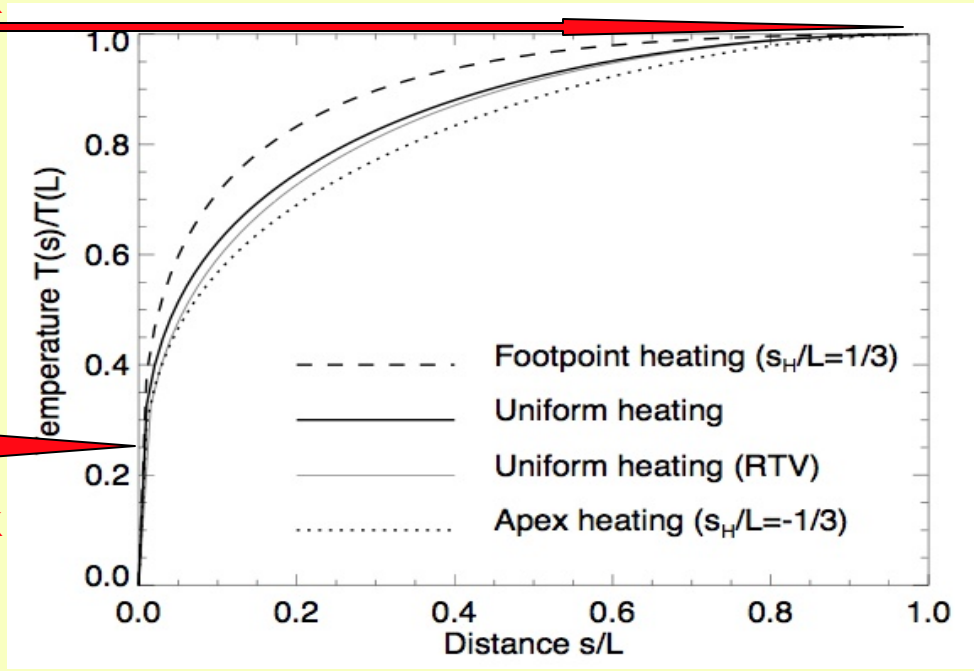

QuickTime™ and a
YUV420 codec decompressor
are needed to see this picture.

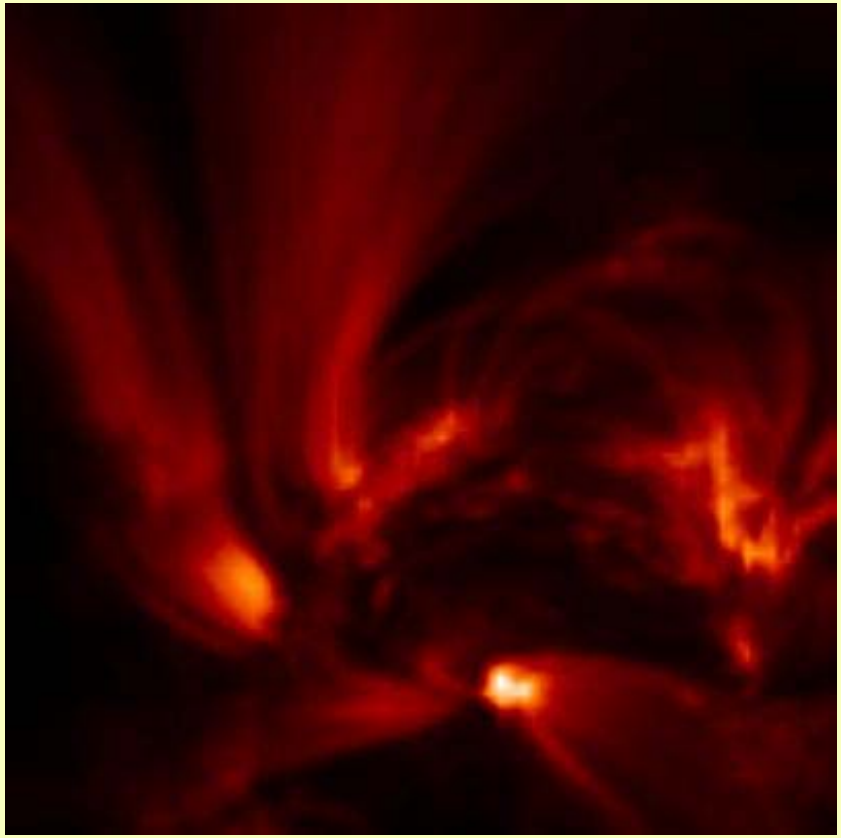

EUVI 171 movie [mgp]

[quicktime.mov, 6 frames/sec]

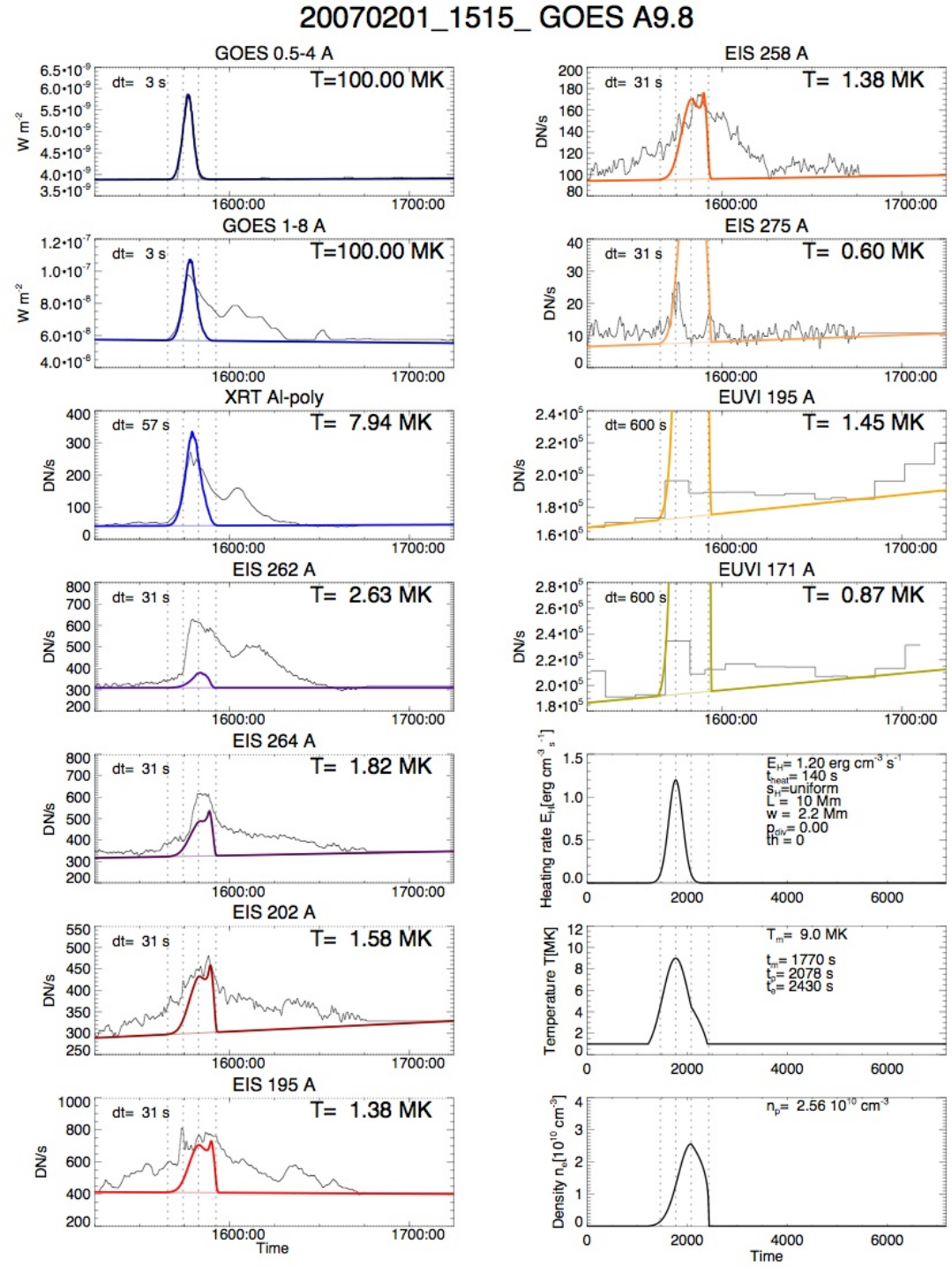

Model fitting GOES, XRT,
EIS 258 A, 195 A, 202 A:

E_H = 1.20 erg cm^{-3} s^{-1}
t_{heat}= 140 s
L = 10 Mm
w = 2.2 Mm

Inconsistent with
EIS 262 A, 264 A, 275 A
And EUVI 171, 195 A

EIS 195 A (T=1.38 MK) is
not consistent with EUVI 195 A
(T=1.45 MK)

<u>Reasons:</u>

- different FOV areas ?
- multi-loop model required ?
- different EUV absorption
  from different aspect angles ?
  (STEREO vs. Hinode)
- Flux calibration ?
- Different time cadence and
  exposure times ?

Example of stereoscopic 3D Reconstruction (2007-May-19, 12:40 UT)

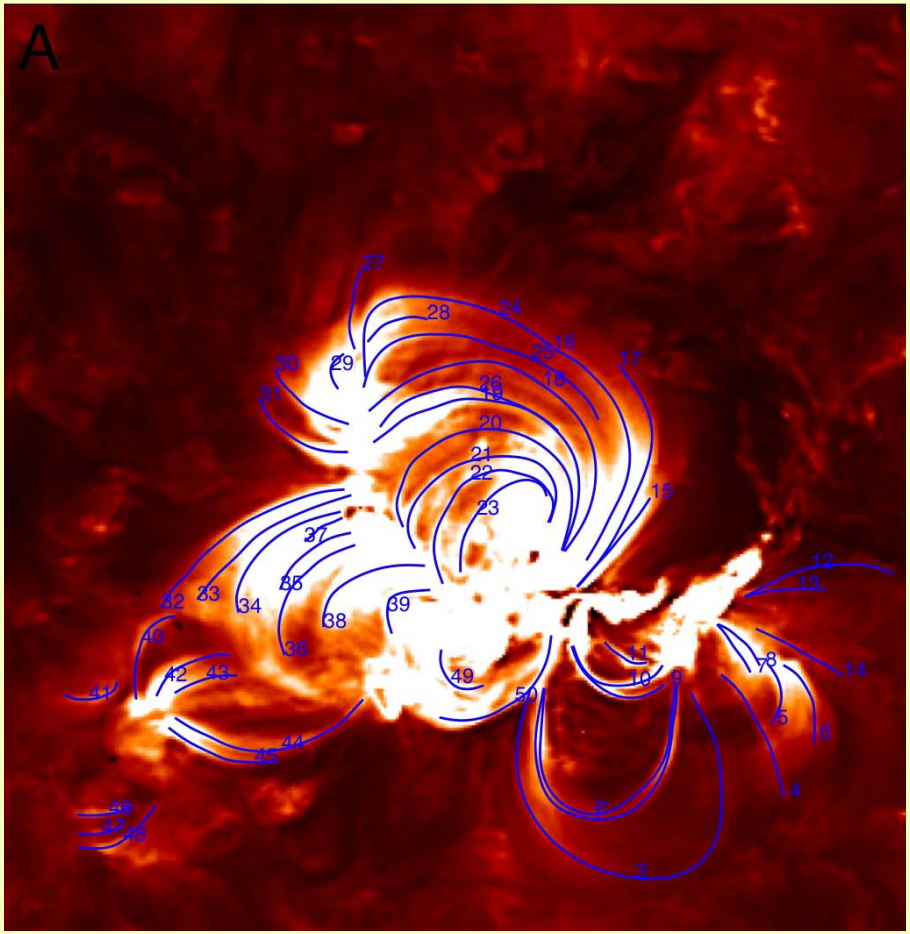

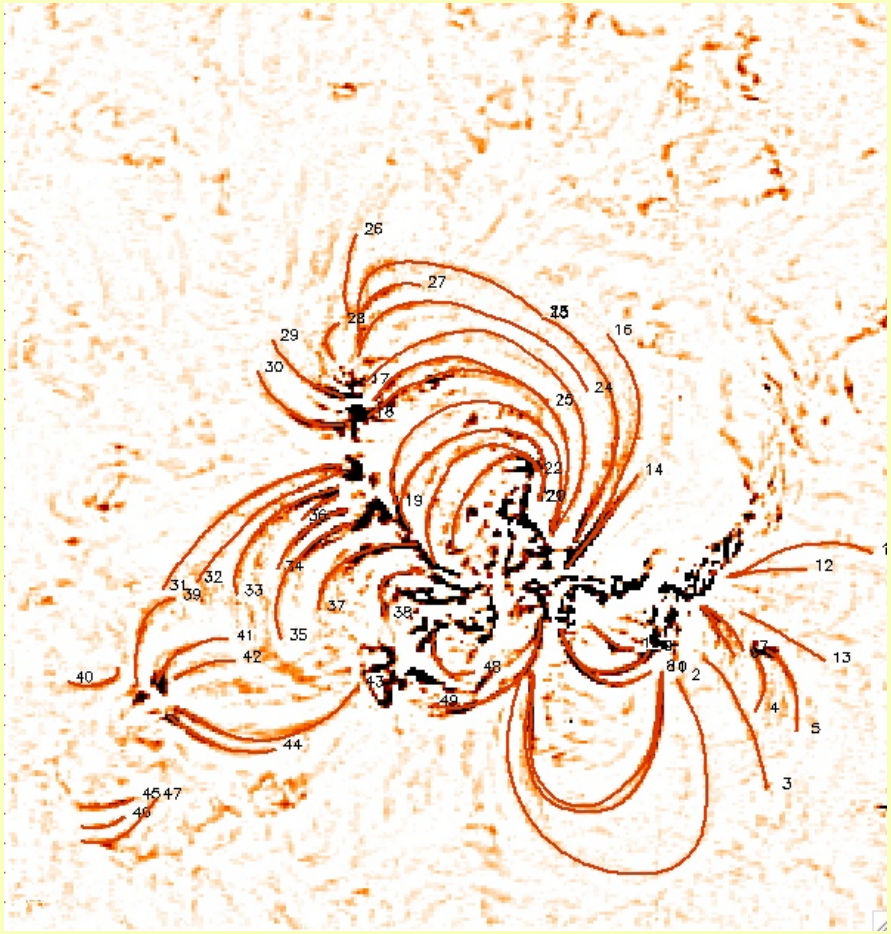

Tracing of 50 loops from high-pass filtered (8 stacked) EUVI image

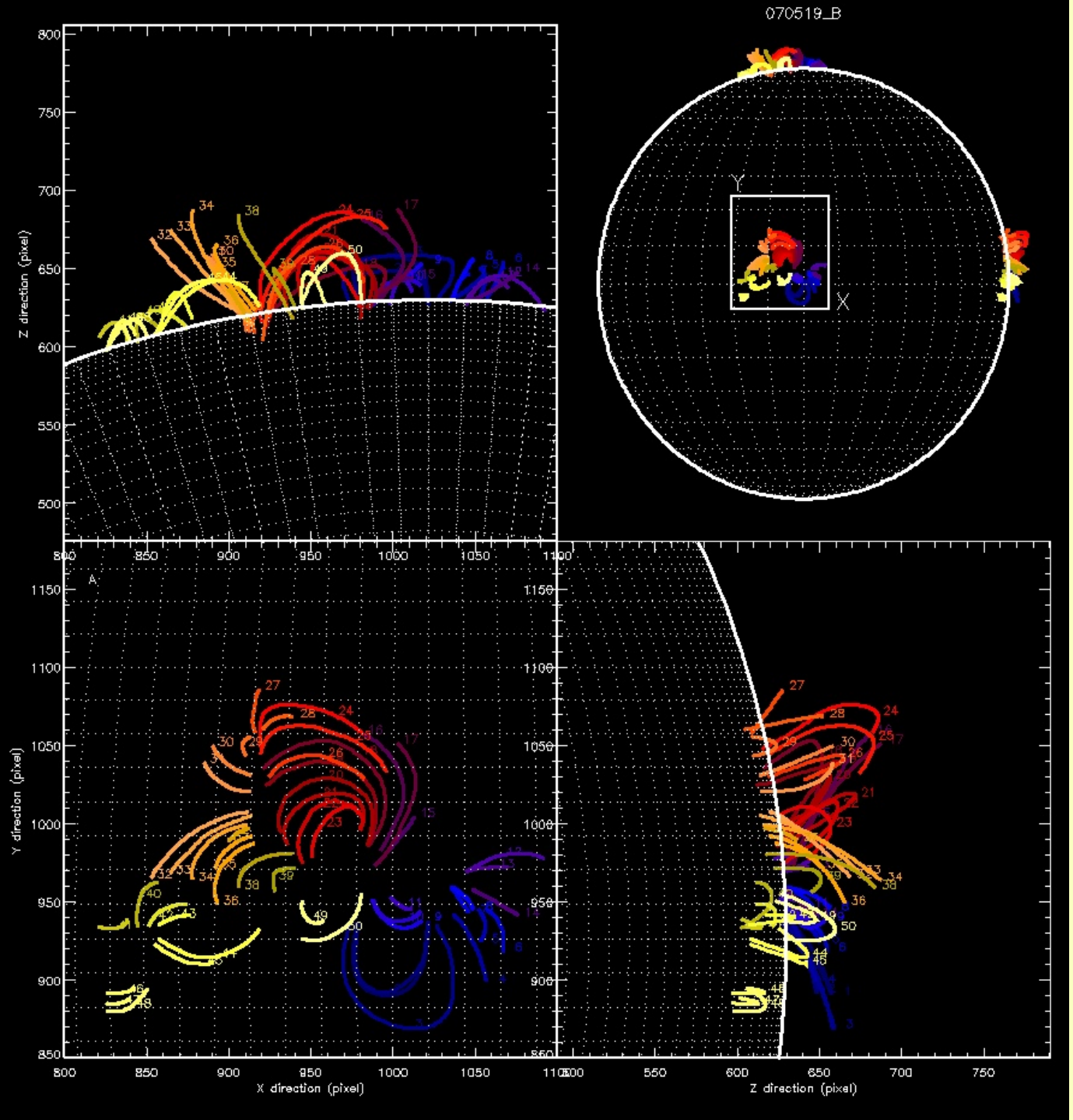

Stereoscopic
Reconstruction
of 3D geometry
of 60 loops
before flare
2007 May 19, 12:40

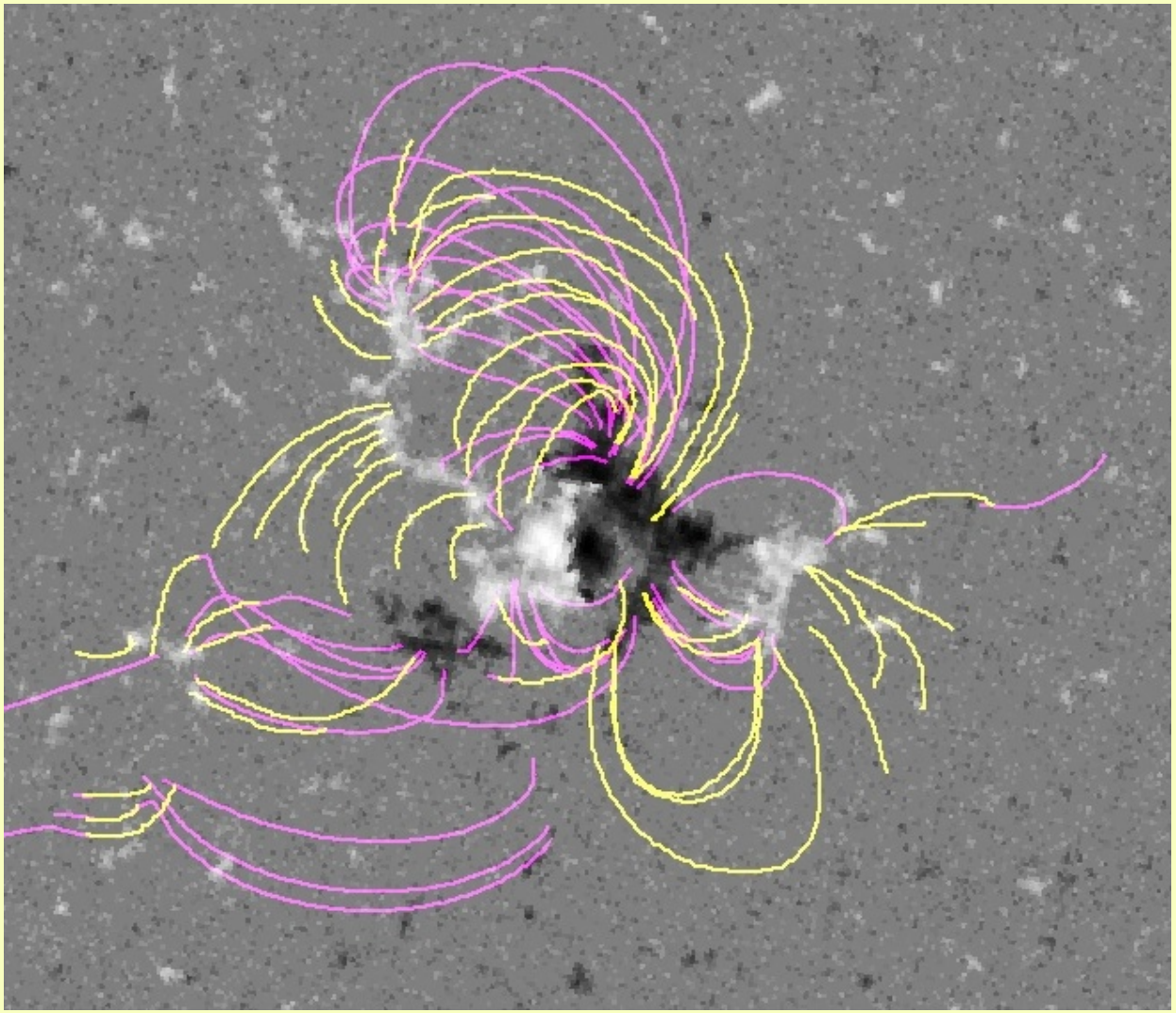

Comparison of EUVI loops traced stereoscopically with “potential field source surface” (PFSS) model extrapolated from SoHO/MDI magnetogram:
--> Note significantly different connectivities !

(courtesy of J.P.Wuelser)

Classical stereoscopy, feasible for small spacecraft separation angles (<45 deg in 2007), yields 3D geometry (skeleton) of AR and 3D vector interpolation yields EUVI-aligned field lines.

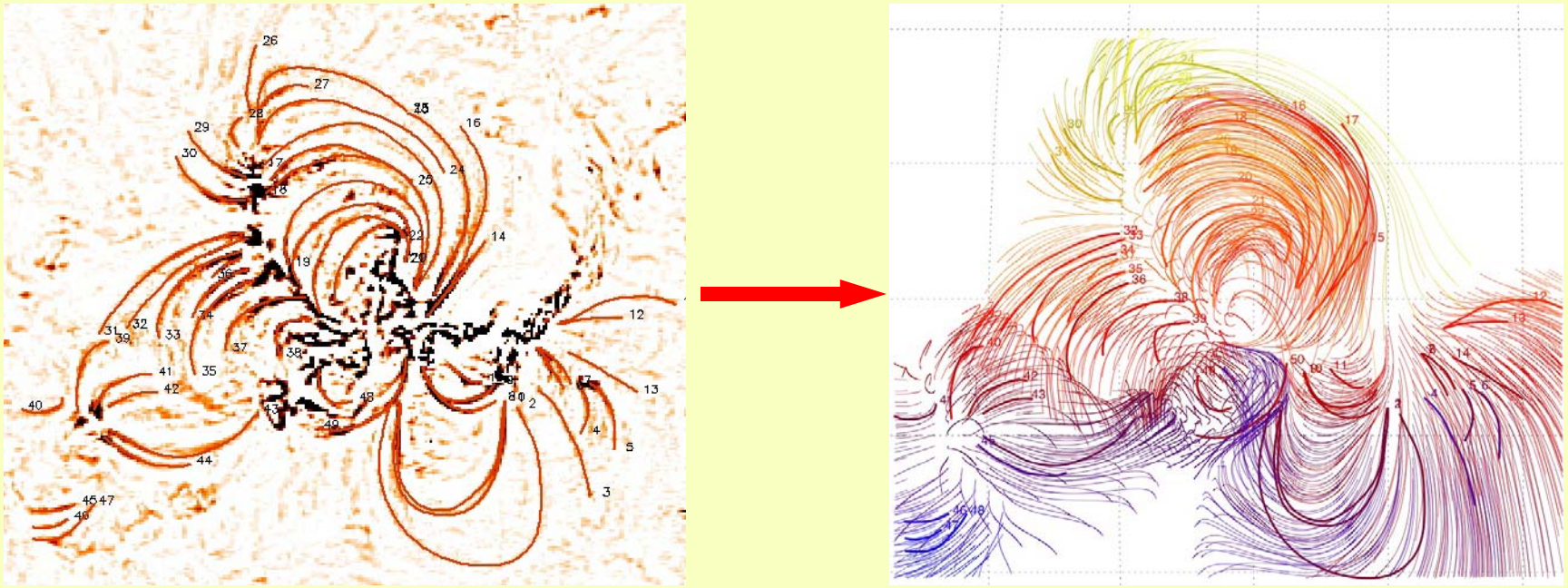

Hydrodynamic forward-modeling of coronal or flare loops renders entire AR/flare regions observed in EUV and soft X-rays. The hydrodynamic non-equilibrium models constrain the spatial and temporal heating function, conductive cooling, and radiative cooling. Stereoscopy provides the loop lengths, inclination angles of loops (to correct hydrostatic scale height), 3D field geometry, DEMs, temperatures, densities, and heating functions.

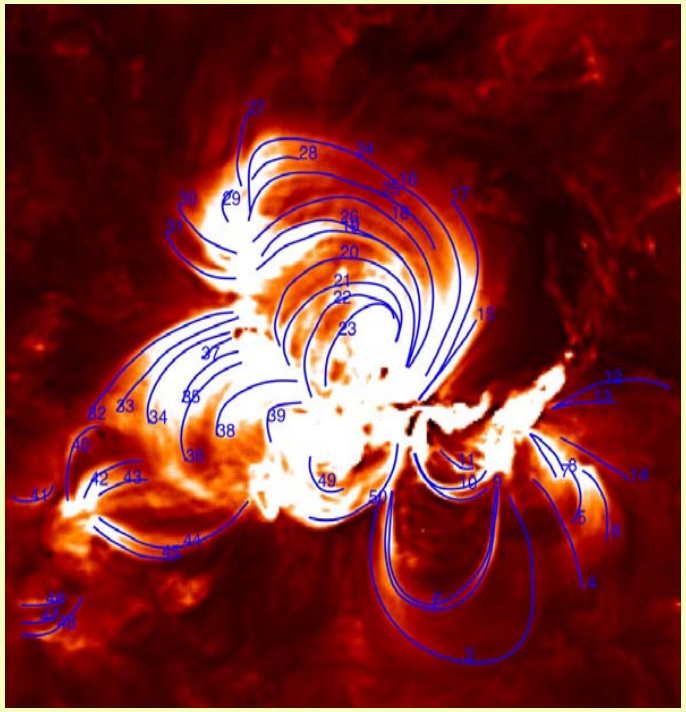

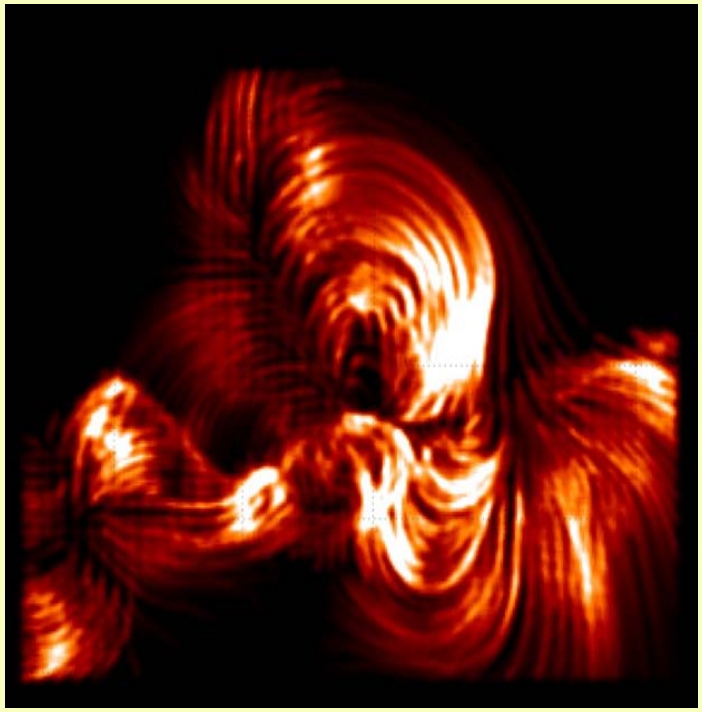

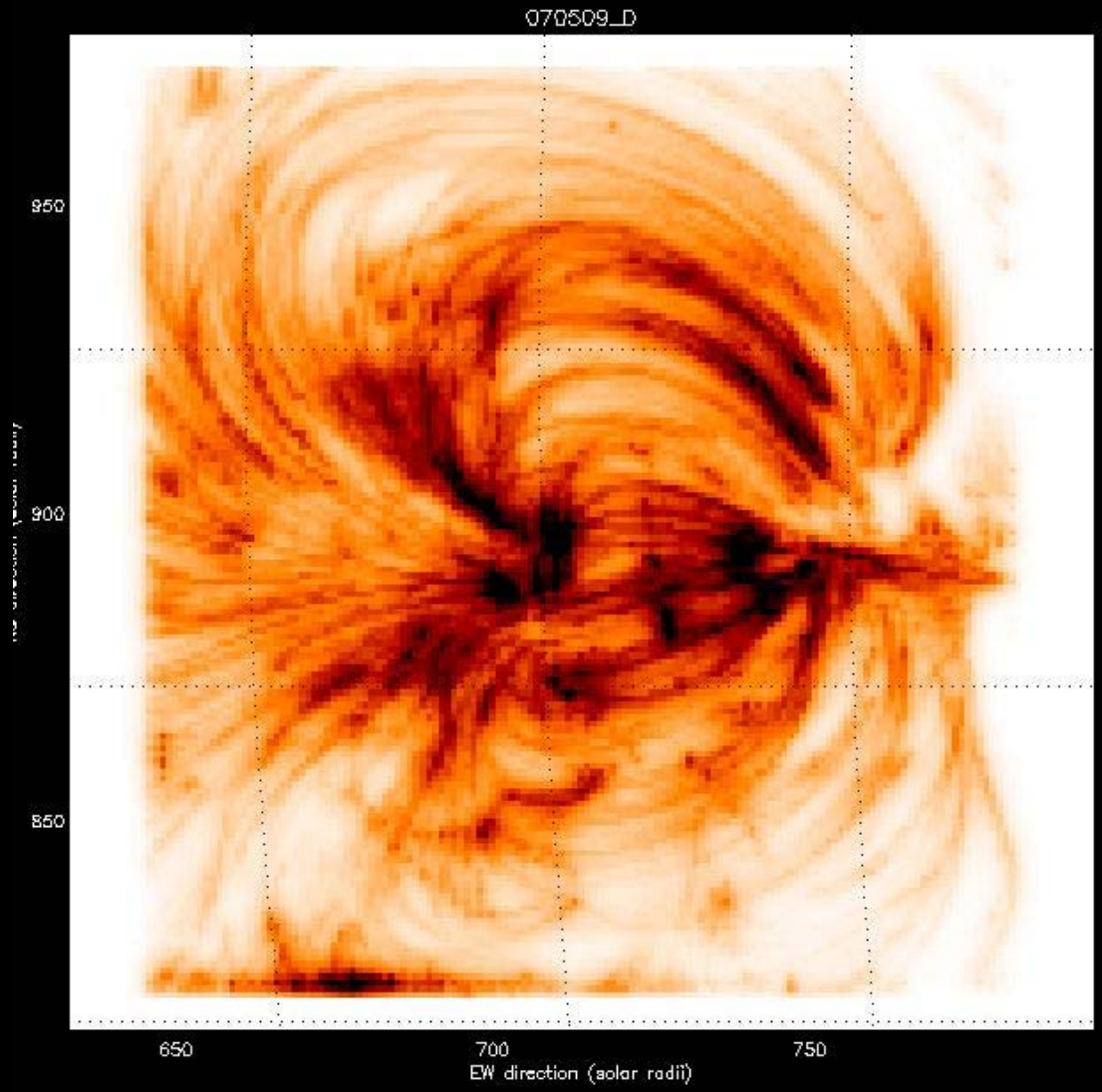
070509_D
950
900
850
650
700
750
EW direction (solar radii)

CONCLUSIONS

(1) Coronal EUV loops observed in EUV are generally not consistent with hydrostatic equlibrium solutions and thus require dynamic modeling.

(2) The hydrodynamic evolution of impulsively heated loops can be analytically approximated by the two phases of (i) dominant (impulsive) haeting (driving chromospheric evaporation into the corona) and (ii) subsequent cooling (by conductive and radiative loss).

(3) The analytical approximations provide a fast forward-fitting method to lightcurves observed in different wavelengths, which in principle allows to constrain the spatio-temporal heating function $E_H(s,t)$. STEREO observations provide 3D geometry of flare/loop systems.

(4) Multi-wavelength modeling of light curves of small flares using GOES, STEREO/EUVI, and Hinode/XRT and EIS observations reveals inconsistencies that need to be further investigated: calibration, FOV, EUV absorption, occultation, multi-loop models…